We are IntechOpen,
the world's leading publisher of
Open Access books
Built by scientists, for scientists

6,900
Open access books available

185,000
International authors and editors

200M
Downloads

154
Countries delivered to

Our authors are among the

TOP 1%
most cited scientists

12.2%
Contributors from top 500 universities

CLARIVATE ANALYTICS
BOOK CITATION INDEX
INDEXED

WEB OF SCIENCE™

Selection of our books indexed in the Book Citation Index
in Web of Science™ Core Collection (BKCI)

Interested in publishing with us?
Contact book.department@intechopen.com

Torque Control of PMSM and Associated Harmonic Ripples

Ali Ahmed Adam[1], and Kayhan Gulez[2]
[1]Fatih University, Engineering Faculty, Electrical-Electronics Eng. Dept., 34500
Buyukcekmece-Istanbul,
[2]Yildiz Technical University, Electrical-Electronics Eng. Faculty, Control and Automation
Engineering Dept., 34349 Besiktas- Istanbul,
Turkey

1. Introduction

Vector control techniques have made possible the application of PMSM motors for high performance applications where traditionally only dc drives were applied. The vector control scheme enables the control of the PMSM in the same way as a separately excited DC motor operated with a current-regulated armature supply where then the torque is proportional to the product of armature current and the excitation flux. Similarly, torque control of the PMSM is achieved by controlling the torque current component and flux current component independently.

Torque Control uses PMSM model to predict the voltage required to achieve a desired output torque or speed. So by using only current and voltage measurements (and rotor position in sensor controled machine), it is possible to estimate the instantaneous rotor or stator flux and output torque demanded values within a fixed sampling time. The calculated voltage is then evaluated to produce switching set to drive the inverter supplying the motor. PMSM torque control has traditionally been achieved using Field Oriented Control (FOC). This involves the transformation of the stator currents into a synchronously rotating d-q reference frame that is typically aligned to the rotor flux. In the d-q reference frame, the torque and flux producing components of the stator current can separately be controlled. Typically a PI controller is normally used to regulate the output voltage to achieve the required torque.

Direct Torque Control (DTC), which was initially proposed for induction machines in the middle of 1980's (Depenbrock, 1984 and 1988; Takahashi, 1986), was applied to PMSM in the late 1990's (French, 1996; Zhong, 1997). In the Direct Torque Control of the PMSM, the control of torque is exercised through control of the amplitude and angular position of the stator flux vector relative to the rotor flux vector. Many methods have been proposed for direct torque control of PMSM among which Hysteresis based direct torque control (HDTC) and Space Vector Modulation direct torque control (SVMDTC).

In 2009 Adam and Gulez, introduced new DTC algortim for IPMSM to improve the performance of hysteresis direct torque control. The algorithm uses the output of two hysteresis controllers used in the traditional HDTC to determine two adjacent active vectors. The algorithm also uses the magnitude of the torque error and the stator flux linkage position to select the switching time required for the two selected vectors. The selection of

the switching time utilizes suggested table structure which, reduce the complexity of calculation. The simulation and experimental results of the proposed algorithm show adequate dynamic torque performance and considerable torque ripple reduction as well as lower flux ripple, lower harmonic current and lower EMI noise reduction as compared to HDTC. Only two hysteresis controllers, current sensors and built-in counters microcontroller are required to achieve torque control.

Torque ripple and harmonic noise in PMSM are due to many factors such as structural imperfectness associated with motor design, harmonics in control system associated with measurement noises, switching harmonics and harmonic voltages supplied by the power inverter which constitute the major source of unavoidable harmonics in PMSM. These harmonics cause many undesired phenomena such as electromagnetic interference "EMI" and torque ripples with consequences of speed oscillations, mechanical vibration and acoustic noise which, deteriorate the performance of the drive in demanding applications (Holtz and Springob 1996). These drawbacks are especially high when the sampling period is greater than 40µs (Zhong, et al. 1997).

Recently many research efforts have been carried out to reduce the torque ripples and harmonics in PMSM due to inverter switching with different degree of success. Yilmaz (Yilmaz, et al. 2000) presented an inverter output passive filter topology for PWM motor drives to reduce harmonics of PMSM, the scheme shows some effectiveness in reducing switching harmonics, but however, very large circulating current between inverter output and filter elements is required to reshape the motor terminal voltage which violate current limitation of the inverter. Many researchers (Hideaki et al, 2000; Darwin et al., 2003; Dirk et al , 2001) have addressed active filter design to reduce or compensate harmonics in supply side by injecting harmonics into the line current which have no effect on the current supplying the load. Satomi (Satomi, et al. 2001) and Jeong-seong (Jeong-seong, et al. 2002) have proposed a suppression control method to suppress the harmonic contents in the d-q control signals by repetitive control and Fourier transform but, however, their work have nothing to do with switching harmonics and voltage harmonics provided by the PWM inverter supplying the motor. Se- Kyo, et al. (1998), Dariusz et al. (2002), and Tang et, al. (2004) have used space vector modulation to reduce torque ripples with good results; however, their control algorithm depends on sophisticated mathematical calculations and two PI controllers to estimate the required reference voltage and to estimate the switching times of the selected vectors. Holtz and Springob (1996, 1998) presented a concept for the compensation of torque ripple by a self- commissioning and adaptive control system.

In this chapter, two different methods to improve torque ripple reduction and harmonic noises in PMSM will be presented. The first method is based on passive filter topology (Gulez et al., 2007). It comprises the effects of reducing high frequency harmonic noises as well as attenuating low and average frequencies. The second method is based on active series filter topology cascaded with two LC filters (Gulez et al., 2008).

Modern PMSM control algorthims

2. Algorithm 1: Rotor Field Oriented Control "FOC"

The control method of the rotor field-oriented PMSM is achieved by fixing the excitation flux to the direct axis of the rotor and thus, it is position can be obtained from the rotor shaft by measuring the rotor angle θ_r and/or the rotor speed ω_r.

Consider the PMSM equations in rotor reference frame are given as:

$$\begin{bmatrix} v_{sd} \\ v_{sq} \end{bmatrix} = \begin{bmatrix} R + pL_{sd} & -P\omega_r L_{sq} \\ P\omega_r L_{sd} & R + pL_{sq} \end{bmatrix} \begin{bmatrix} i_{sd} \\ i_{sq} \end{bmatrix} + \begin{bmatrix} 0 \\ P\omega_r \psi_F \end{bmatrix} \qquad T_e = \frac{3}{2} P(\psi_F i_{sq} + (L_{sd} - L_{sq}) i_{sd} i_{sq})) \tag{1}$$

Where,

v_{sd}, v_{sq}: d-axis and q-axis stator voltages;

i_{sd}, i_{sq}: d-axis and q-axis stator currents;

R: stator winding resistance;

L_{sd}, L_{sq}: d-axis and q-axis stator inductances;

$p=d/dt$: differential operator;

P: number of pole pairs of the motor;

ω_r: rotor speed;

Ψ_F: rotor permanent magnetic flux;

Te: generated electromagnetic torque;

To produce the largest torque for a given stator current, the stator space current is controlled to contain only i$_{sq}$.

And since for PMSM $L_d \leq L_q$, the second torque component in Eq.(1) is negative with positive values of i$_{sd}$ and zero for SPMSM. Thus, to ensure maximum torque, the control algorithm should be such that i$_{sd}$ is always zero, which result in simple torque expression as:

$$T_e = 3/2 \ P \ \psi_F \ i_{sq} = 3/2 \ \psi_F | \ i_s| \ sin(\alpha - \theta_r) \tag{2}$$

The stator windings currents are supplied from PWM inverter, using hysteresis current controller. The actual stator currents contain harmonics, which, produce pulsating torques, but these may be filtered out by external passive and active filters, or using small hysteresis bands for the controllers.

2.1 Implementation of rotor field oriented control

The block diagram of rotor-field oriented control of PMSM in polar co-ordinate is shown in Fig.1 (Vas, 1996). The stator currents are fed from current controlled inverter. The measured stator currents are transformed to stationary D-Q axis. The D and Q current components are then transformed to polar co-ordinate to obtain the modulus $|i_s|$ and the phase angle α_s of the stator-current space phasor expressed in the stationary reference frame.
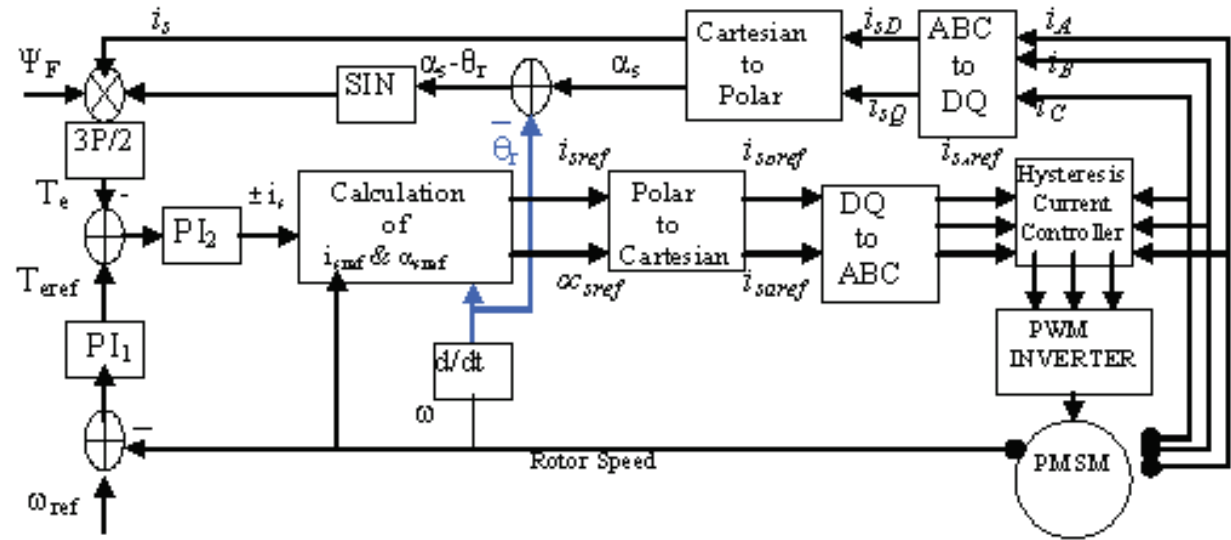

Fig. 1. Rotor Field Oriented Control of PMSM

The rotor speed ω_r and rotor angle θ_r are measured; and the position of the stator current in the rotor reference frame is obtained. Then, the instantaneous electromagnetic torque *Te* can be obtained as stated in Eq. (2).

The necessary current references to the PWM inverter are obtained through two cascaded PI controllers. The measured rotor speed ω_r is compared with the given reference speed ω_{ref} and the error is controlled to obtained the reference torque T_{eref}. The calculated torque is subtracted from the reference torque and the difference is controlled to obtain the modulus of i$_{sref}$. The reference angle α_{sref} is set equal to $\pi/2$, and the actual rotor angle is added to ($\alpha_{sref} - \theta_r$) to obtain the angle α_{sref} of the stator current in the stationary D-Q frame. Theses values are then transformed to the three-reference stator currents i_{sAref}, i_{sBref} and i_{sCref} and used to drive the current controller.

The functions of the PI controllers (other controllers such as Fuzzy Logic, Adaptive, Slide mode or combinations of such controller may be used) are to control both the speed and torque to achieve predetermined setting values such as:

1. Zero study state error and minimum oscillation,
2. Wide range of regulated speed,
3. Short settling time,
4. Minimum torque ripples,
5. Limited starting current.

Based on the above description a FOC model was built in MatLab/Simulink as shown in Fig. 2. The model responses for the data setting in Table 1 of SPMSM with ideal inverter were displayed in Fig.3 to Fig.7. The PI controllers setting and reference values are:

Ts=1 µs, ω_{ref} =300, T$_L$ =5Nm,   PI$_2$: Kp=10, Ki=0.1 PI$_1$: Kp=7, Ki=0.1.
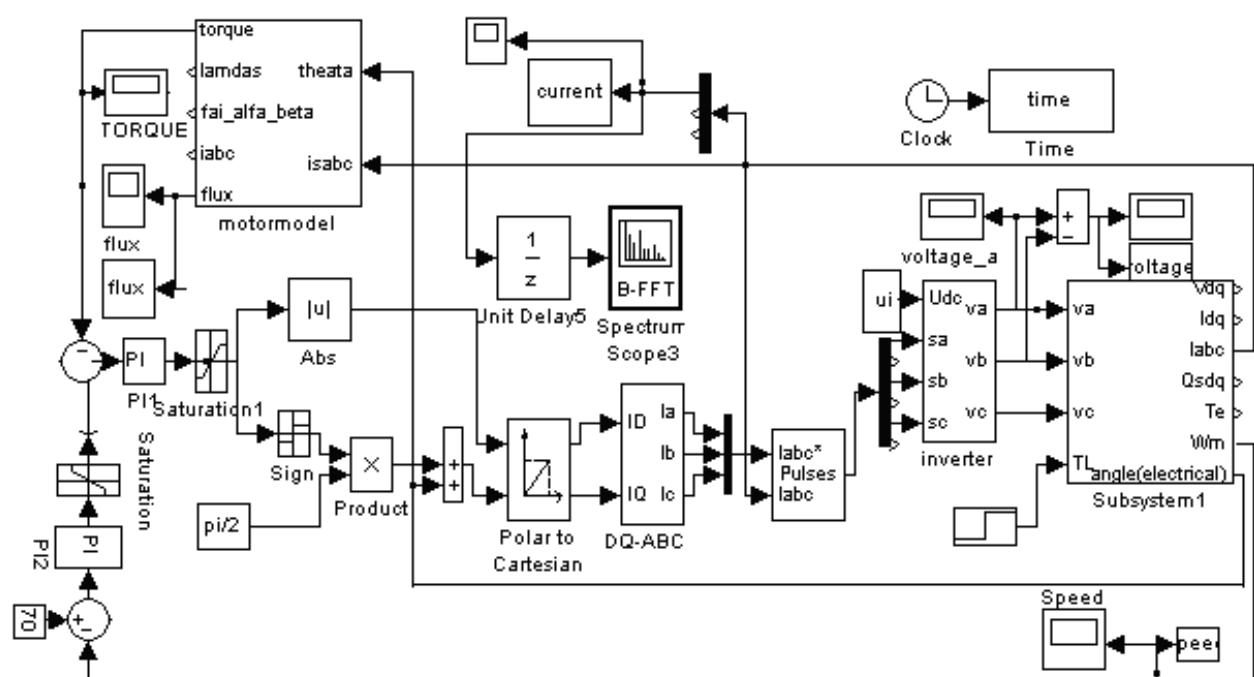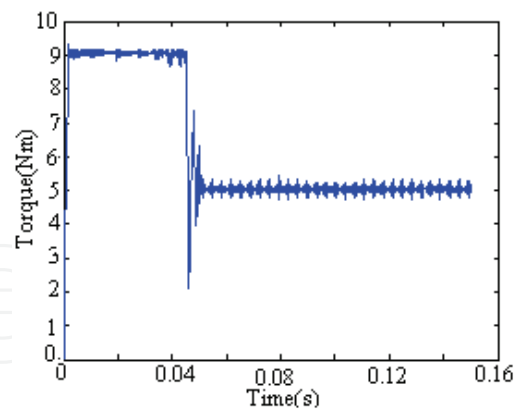

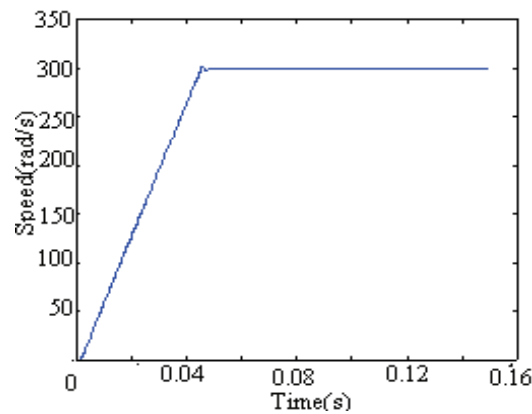Fig. 2. FOC model in Matlab/Simulink
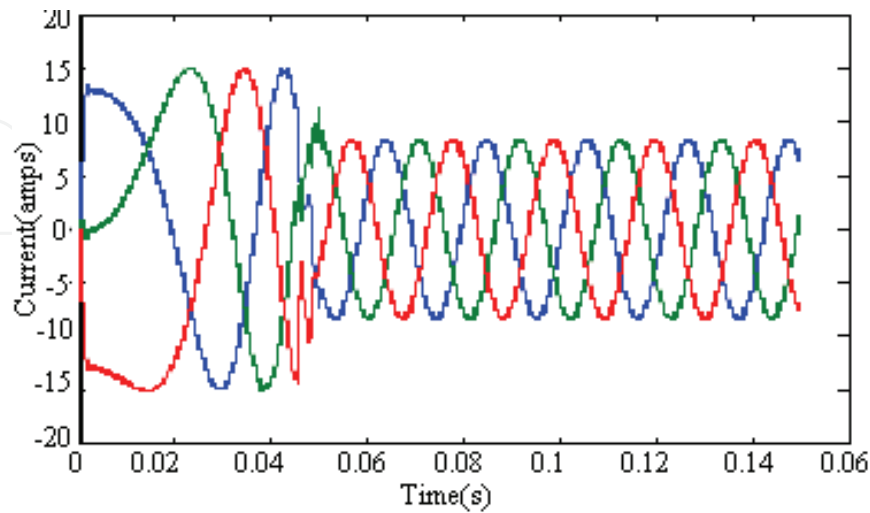
Fig. 3. Torque response

Fig. 4. Speed response
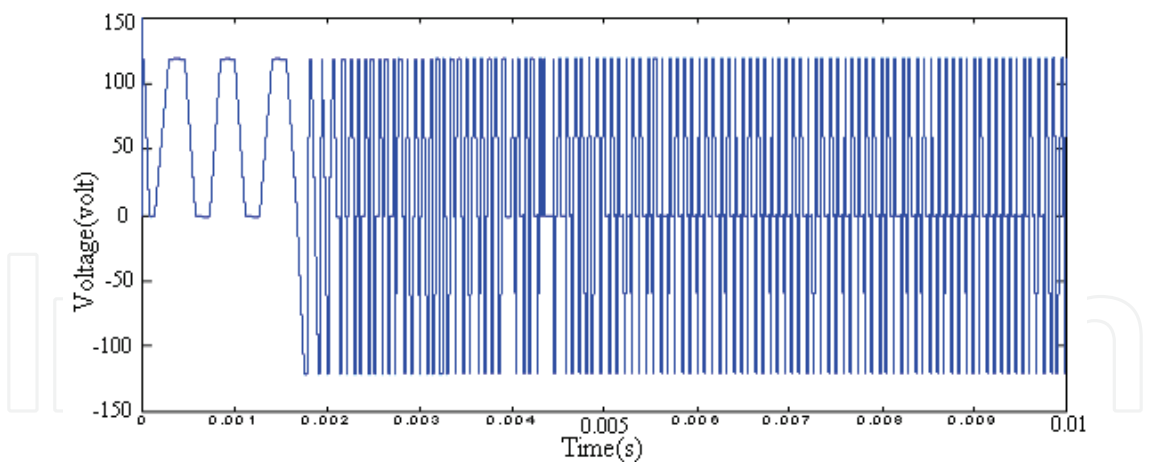

Fig. 5. Line current response
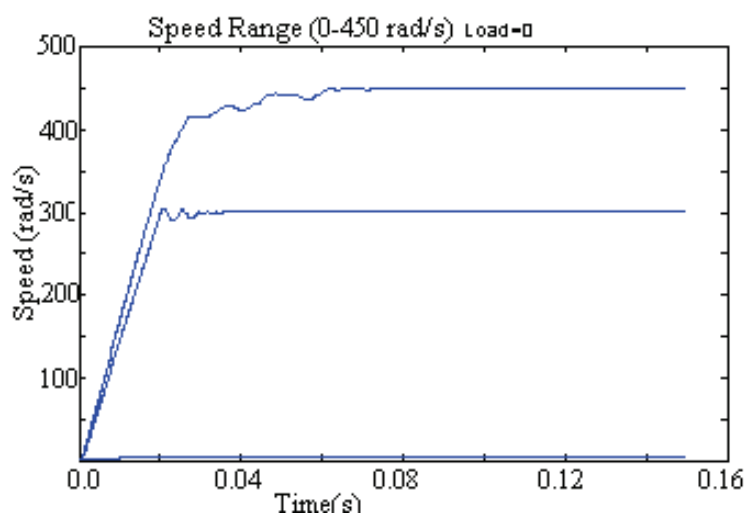
Fig. 6. V$_{ab}$ switching pattern

Fig. 7. Regulated Speed range (0-450) rad/s

Vdc	120V
Ψ_F	0.1546 web.
Rs	1.4 ohm
Ld	0.0066 H
Lq	0.0066 H
J	0.00176 kGm²
B	0.000388 N/rad/s

Table 1. Motor parameters

The above figures show acceptable characteristics however, the torque pulsation cannot be avoided and the line currents are almost sinusoidal with some harmonic values. The speed can be regulated up to the rated value (300rad/s) with acceptable response. Bearing in mind that sensors, analog/digital converters, switching elements of the inverter and algorithm

processing in DSP are time consuming, it is practically difficult to achieve such system with small sampling period. Thus, in practice convenient sampling periods, such as 100 µs (or larger) is normally selected for processing. In the following, simulation practical values will be adopted to obtain reasonable results for comparison. So, PMSM with parameters shown in Table 2 was simulated in the same model with the following setting values:

Ts=100 µs, T_L =2Nm, ω_{ref} =70 rad/s   PI$_2$: Kp=10, Ki=0.1 and PI$_1$: Kp=7, Ki=0.1

Number of pole pairs	P	2
Stator leakageresistance	R_s	5.8 Ohm
d-axis inductance	L_{sq}	102.7 mH
q-axis inductance	L_{sd}	44.8 mH
Permanent magnet flux	Ψ_F	533 mWb
Inertia constant	J	0.000329Nms^2
Friction constant	B	0.0
Reference speed	ω	70 rad/s
Load torque	T_L	2 Nm

Table 2. IPMSM parameters
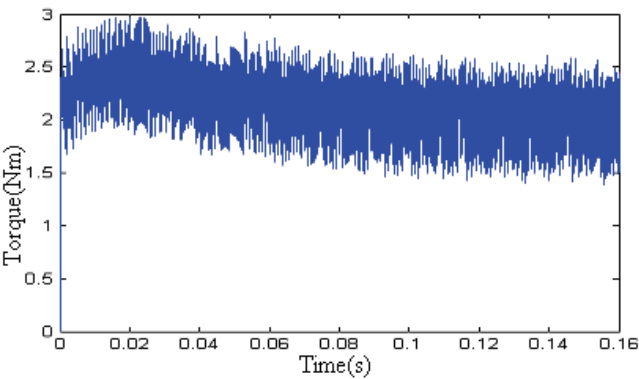
The simulation responses were shown below:
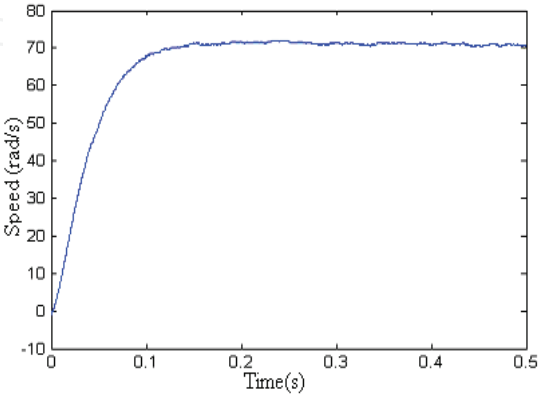

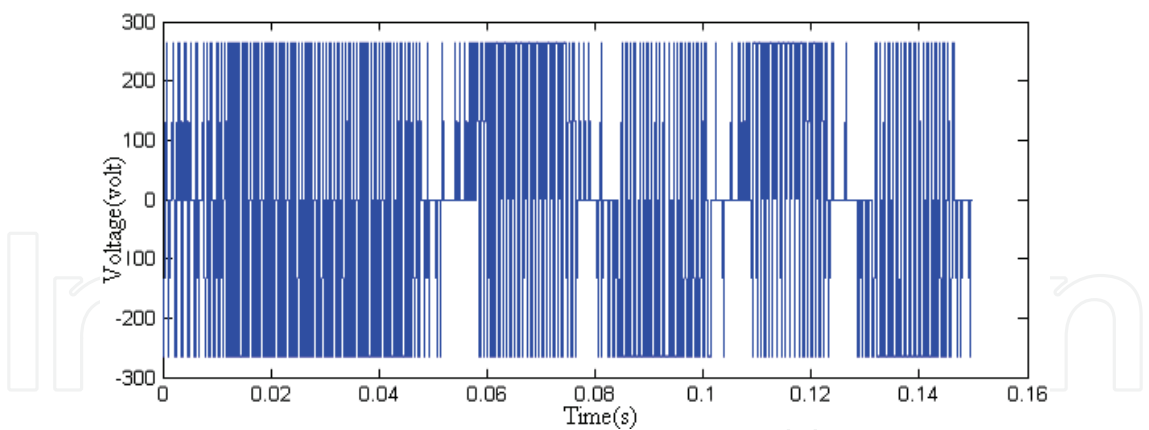Fig. 8. FOC Torque response

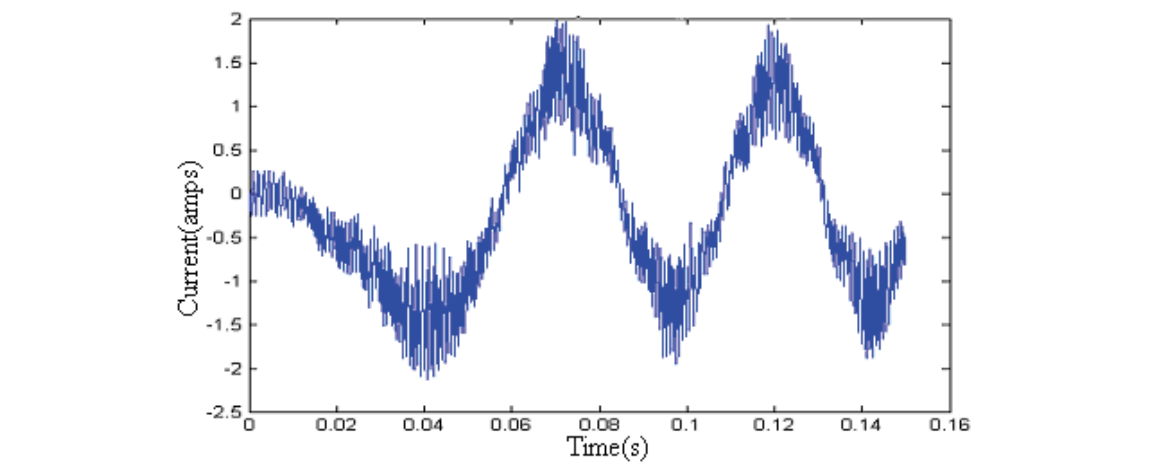Fig. 9. FOC Speed response

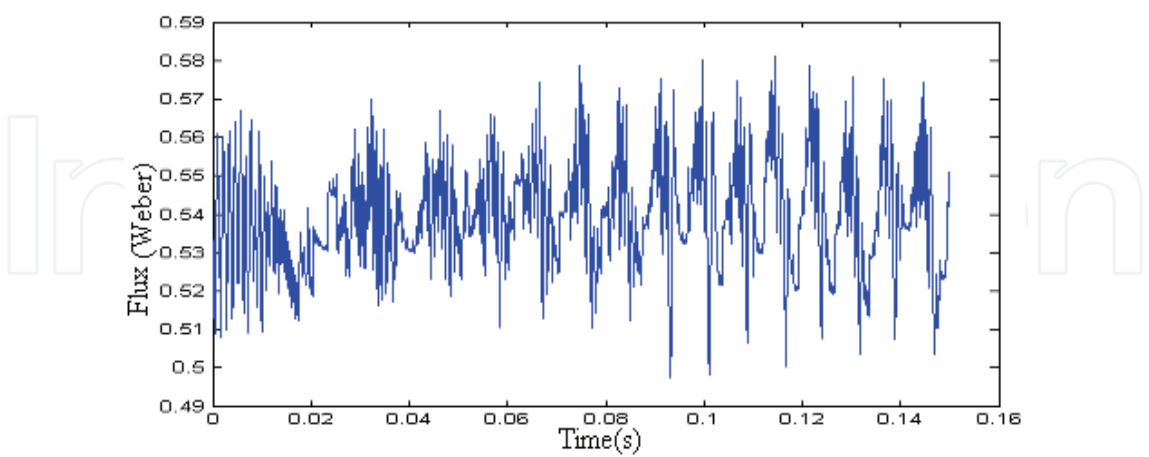Fig. 10. FOC Line Voltage Switching

Fig. 11. FOC Current response

Fig. 12. Flux response

The responses showed that the torque pulsation is very high and line currents are full of harmonic components which give rise to EMI noises, in addition flux and speed are not free of ripples which result in unwanted phenomena such as machine vibration and acoustic noise.

3. Algorithm 2: Hysteresis Direct Torque Control (HDTC)

This method which is also called Basic DTC can be explained by referring to Fig.13. In this figure, the angle between the stator and rotor flux linkages δ is the load angle when the stator resistance is neglected. In the study, state δ is constant corresponds to a load torque, where stator and rotor flux rotate at synchronous speed. In transient operation, δ varies and the stator and rotor flux rotate at different speeds. Since the electrical time constant is normally much smaller than the mechanical time constant, the rotating speed of stator flux with respect to rotor flux, can easily be changed also that the increase of torque can be controlled by controlling the change of δ or the rotating speed of the stator flux (Zhong, 1997) as will be explained in the following analysis.
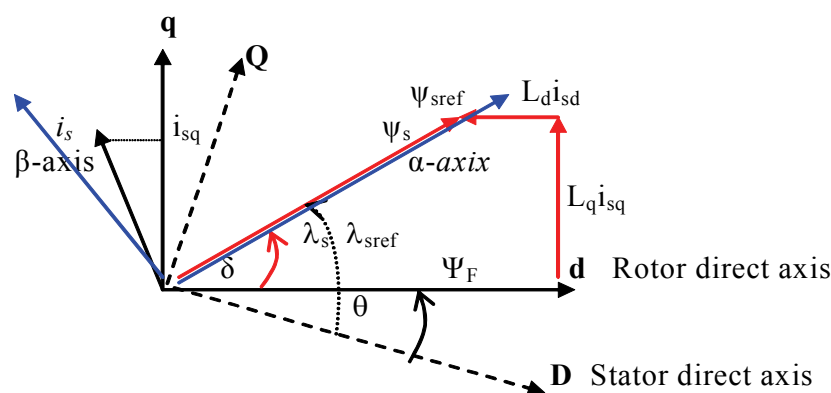

Fig. 13. Stator and rotor flux space phasors

3.1 Flux and torque criteria
Referring to Fig. 13 the flux equations in rotor dq axis frame can be rewritten as:

$$\psi_{sd} = L_{sd}i_{sd} + \psi_F = |\psi_s|\cos\delta \tag{3}$$

$$\psi_{sq} = L_{sq}i_{sq} = |\psi_s|\sin\delta \tag{4}$$

Where, $|\psi_s|$ represent the amplitude of the stator flux linkage calculated as:

$$\left|\bar{\psi}_s\right|^2 = \left(L_{sd}i_{sd} + \psi_F\right)^2 + \left(L_{sq}i_{sd}\right)^2 \tag{5}$$

In the general α-β reference frame the torque equation can be written as (Zhong, 1997):

$$T_e = \frac{3}{2}P|\psi_s|i_{s\beta} \tag{6}$$

Where; i_β is the component of the stator phasor space current perpendicular to the stator flux axis α.
Equation (6) suggests that the torque is directly proportional to the β-axis component of the stator current if the amplitude of the stator flux linkage is kept constant.
Now using Eq.(3) and Eq.(4) to rewrite the torque equation as:

$$T_e = \frac{3P|\psi_s|}{4L_{sd}L_{sq}}\left[2\psi_F L_{sq}\sin\delta - |\psi_s|\left(L_{sq}-L_{sd}\right)\sin 2\delta\right] \qquad (7)$$

For SPMSM $L_{sd} = L_{sq} = L_s$ and this expression is reduced to

$$T_e = \frac{3P|\psi_s|}{2L_s}\psi_F\sin\delta = \frac{3P|\psi_s|}{2L_s}\psi_F\sin\delta^\bullet t \qquad (8)$$

Where $\delta^\bullet$ is the angular speed of the stator flux linkage relative to the permanent magnet axis.

At constant flux values, Eq. (8) shows that T_e-δ has sinusoidal relationship and the derivative of this equation suggest that the increase of torque is proportional to the increase of δ in the range of $-\pi/2$ to $\pi/2$. So the stator flux linkage should be kept constant and the rotational speed $\delta^\bullet$ is controlled as fast as possible to obtain the maximum change in actual torque.

For IPMSM, the torque expression contains in addition to the excitation torque, reluctance torque and for each stator flux level value, there exist different T_e-δ curve and different maximum torque. Fig. 14 (Zhong, 1997) shows these relationship for different values of $|\psi_s|$. Observe the crossing of curve $|\psi_s|=2\psi_F$ where, the derivative of torque near zero crossing has negative value, which implies that DTC can not be applied in this case.
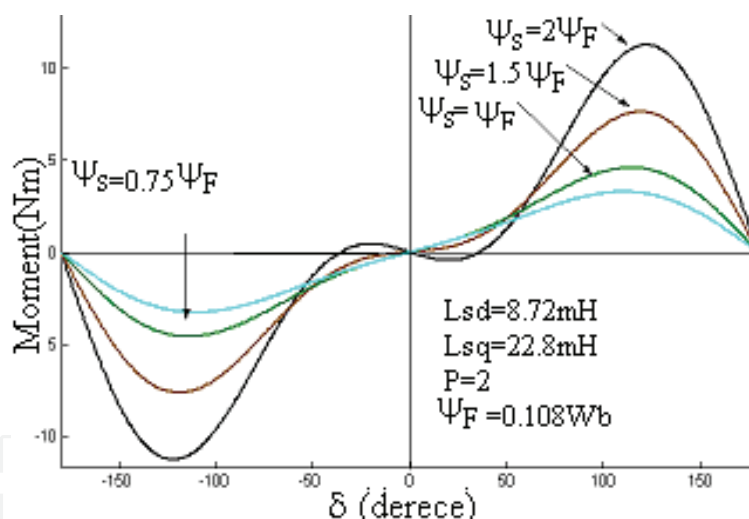

Fig. 14. Different T_e-δ curves for different stator flux values

Analytically this condition can be obtained from derivative of Eq. (7) as follows:

$$\frac{dT_e}{dt} = \frac{3P|\psi_s|}{2L_{sd}L_{sq}}\left[\psi_F L_{sq}\delta^\bullet - |\psi_s|\left(L_{sq}-L_{sd}\right)\delta^*\right] \qquad (9)$$

And thus for positive torque derivative under positive $\delta^\bullet$, $|\psi_s|$ should be selected in such a way that (Tang et al., 2002; Zhong et al. 1997):

$$|\psi_s| \langle \frac{L_{sq}}{L_{sq}-L_{sd}}\psi_F \qquad (10)$$

That if fast dynamic response is required. Also that (Tang et al., 2002) for stable torque control the following criteria should be satisfied.

$$\delta < \cos^{-1}(\frac{a/\psi_s - \sqrt{(a/\psi_s)^2 + 8}}{4})\quad\quad\quad(11)$$

Where, a = $\dfrac{L_{sq}}{L_{sq} - L_{sd}}\psi_F$

3.2 Control of stator flux strategy

The stator flux linkage of a PMSM in the stationary reference frame can be expressed as:

$$\psi_s = \int(V_s - Ri_s)dt = V_s t - R\int i_s dt + \psi_s\big|_{t=0}\quad\quad\quad(12)$$

During switching interval each voltage vector is constant, so if stator resistance is neglected then, this equation implies that the stator flux will move in the direction of the applied voltage vector.

To select the voltage vectors or controlling the amplitude of the stator flux linkage, the voltage vector plane is divided into six sectors (FS_1 to FS_6) as shown in Fig. 15. In each region two adjacent voltage vectors are selected to increase or decrease the amplitude respectively of the flux within a hysteresis band. For example, the vectors V_2 and V_3 are used to increase and decrease the flux amplitude when ψ_s is in region one and rotating in a counter clockwise direction. If rotating in clockwise direction then V5 and V6 are used for the same reason.
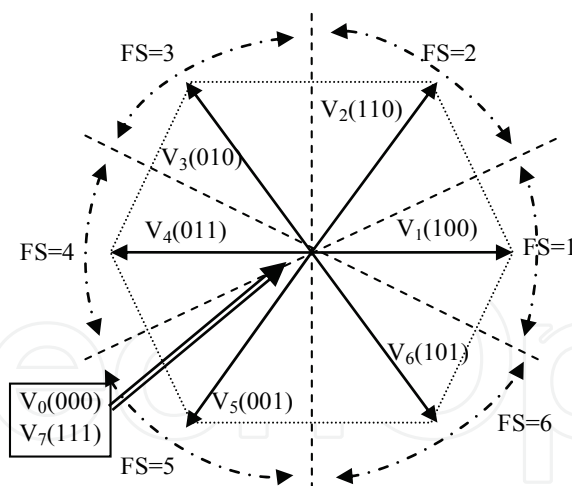

Fig. 15. Applied vectors position and flux sectors.

3.3 Implementation of Hysteresis DTC

The block diagram of a PMSM drive with HDTC may be as shown in Fig. 16, where the measured current phase values and dc voltage are transferred to D-Q stationary axis values, and the flux linkage components ψ_{sD} and ψ_{sQ} at the mth sampling instance are calculated from the stator voltages as follows:

$$\psi_{sD}(m) = \psi_{sD}(m-1) + (V_D(m-1) - Ri_{sD})Ts\quad\quad\quad(13)$$

$$\psi_{sQ}(m) = \psi_{sQ}(m-1) + (V_Q(m-1) - Ri_{sQ})Ts \qquad (14)$$

Where Ts is the sampling period and i_{sD} and i_{sQ} are calculated as average values of $i_s(m-1)$ and $i_s(m)$ and thus, amplitude and flux angle position with respect to stationary D-Q axis can be calculated as:

$$|\psi_s| = \sqrt{\psi_D^2(m) + \psi_Q^2(m)}$$
$$\lambda_s = \tan^{-1}\frac{\psi_Q(m)}{\psi_D(m)} \qquad (15)$$

The torque can be rewritten in the stationary reference frame as (Zhong et al., 1997):

$$T_e(m) = \frac{3}{2}P\left(\psi_{sD}(m)i_{sQ}(m) - \psi_{sQ}(m)i_{sD}(m)\right) \qquad (16)$$

However if the phase currents and the rotor speed and/or rotor position are monitored then Eq. (3) and Eq. (4) can be used to calculate torque and flux values, where then the transformation D-Q ↔ d-q is necessary to achieve the required values.
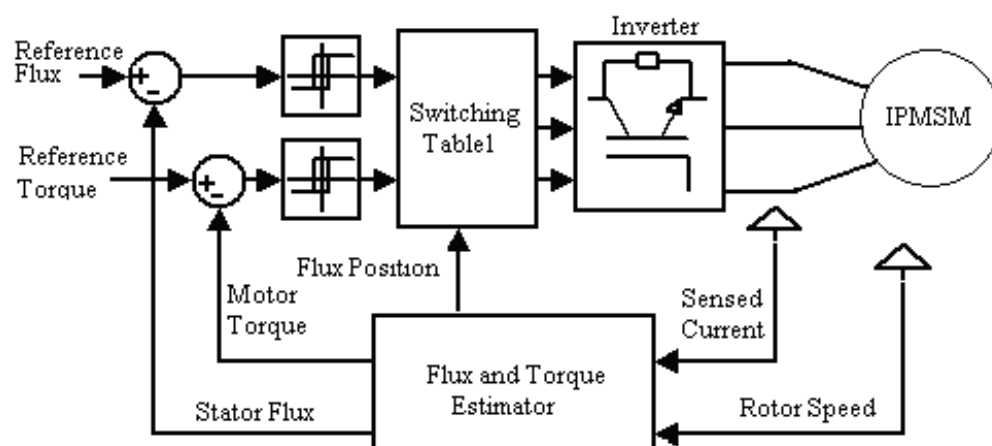

Fig. 16. HDTC of PMSM

The calculated Torque and Flux magnitude values are compared with their respective reference values and the produced errors are inputs to their respective hysteresis comparators. The flux linkage comparator is a two level comparator $\phi\,\varepsilon\,\{1, 0\}$ and the torque comparator is a three level comparator $\tau\,\varepsilon\{1, 0, -1\}$. The outputs of these comparators together with stator position λ_s (or sector number) are inputs to optimum voltage switching lookup table as the one shown in Table 3 (Luukko, 2000). The output of this table is switching vector to the inverter driving the motor.

Based on the above description a HDTC of PMSM model was built in Matlab Simulink as shown in Fig.17.

The torque and flux estimator is based on monitoring of phase currents and rotor angle. The model responses for the Table 2 and controllers setting values as:

PI speed controller: Kp=0.04 and Ki=2,

Hysteresis logic: Flux band = ± 0.01; Torque Band = ±0.01; Sampling time: Ts= 0.0001s; has been simulated with results displayed in Fig.18-Fig.22

Φ	τ	FS					
		1	2	3	4	5	6
		$-30 \leq \lambda_s < 30$	$30 \leq \lambda_s < 90$	$90 \leq \lambda_s < 150$	$150 \leq \lambda_s < 210$	$210 \leq \lambda_s < 270$	$270 \leq \lambda_s < 330$
1	1	$V_2(110)$	$V_3(010)$	$V_4(011)$	$V_5(001)$	$V_6(101)$	$V_1(100)$
	0	$V_7(111)$	$V_0(000)$	$V_7(111)$	$V_0(000)$	$V_7(111)$	$V_0(000)$
	-1	$V_6(101)$	$V_1(100)$	$V_2(110)$	$V_3(010)$	$V_4(011)$	$V_5(001)$
0	1	$V_3(010)$	$V_4(011)$	$V_5(001)$	$V_6(101)$	$V_1(100)$	$V_2(110)$
	0	$V_0(000)$	$V_7(111)$	$V_0(000)$	$V_7(111)$	$V_0(000)$	$V_7(111)$
	-1	$V_5(001)$	$V_6(101)$	$V_1(100)$	$V_2(110)$	$V_3(010)$	$V_4(011)$

Table 3. Optimum switching lookup table for HDTC inverter. Φ is the output of flux hysteresis controller, τ is the output of the torque hysteresis controller, the entries $V_i(...)$ is the switching logic to the inverter and FS (Flux Sector) define the stator flux position sector
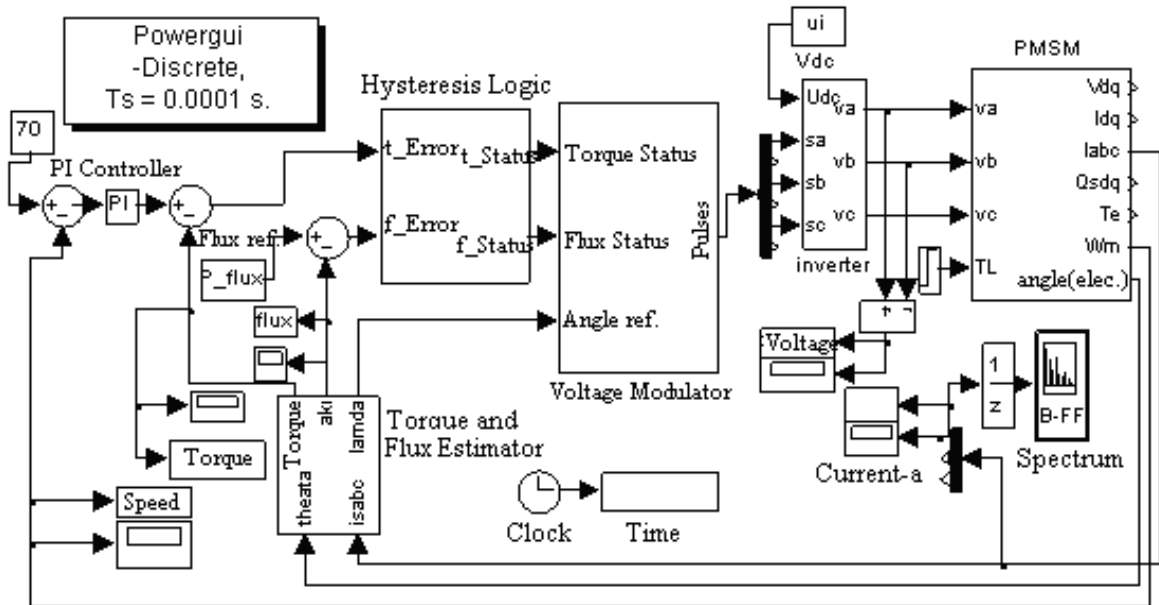

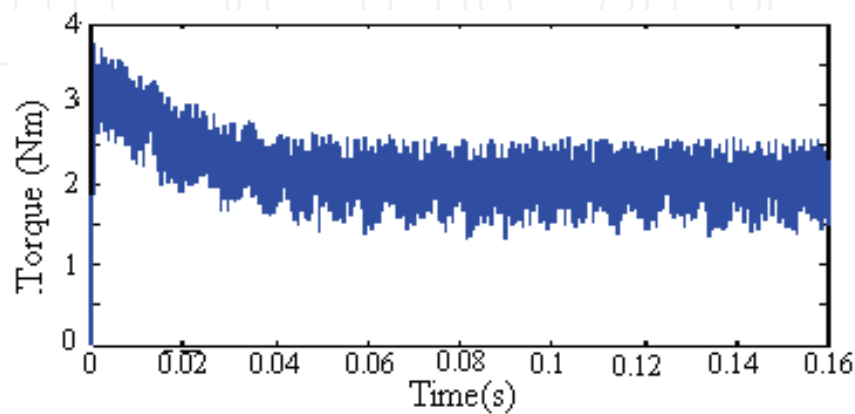
Fig. 17. HDTC of PMSM in Matlab/Simulink
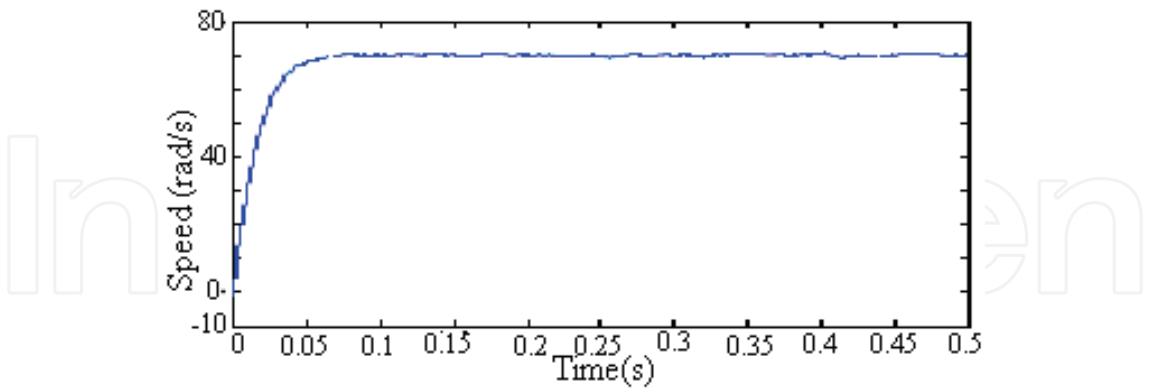

Fig. 18. Torque Response
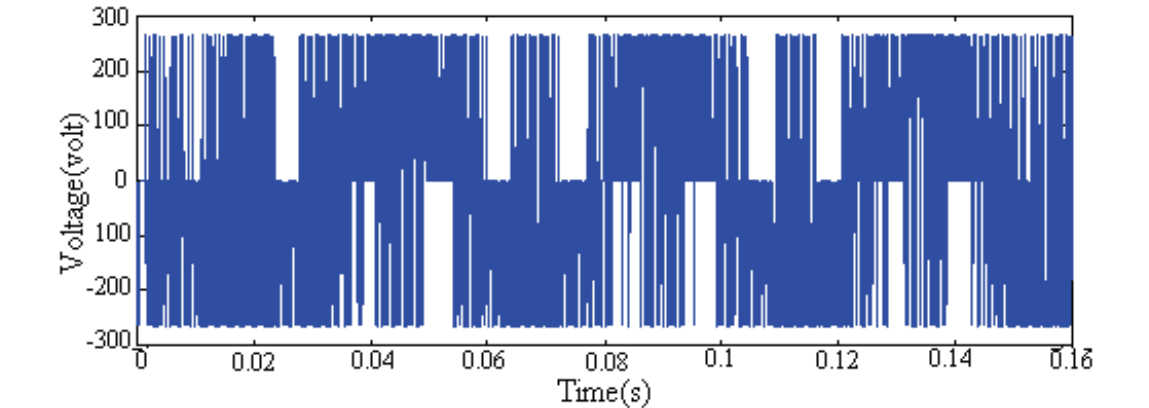
Fig. 19. Speed Response
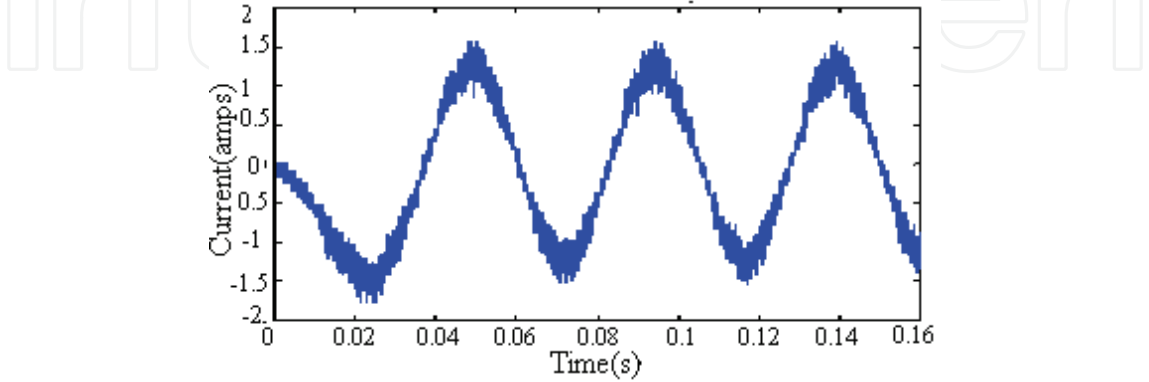

Fig. 20. Voltage switching of line a-b
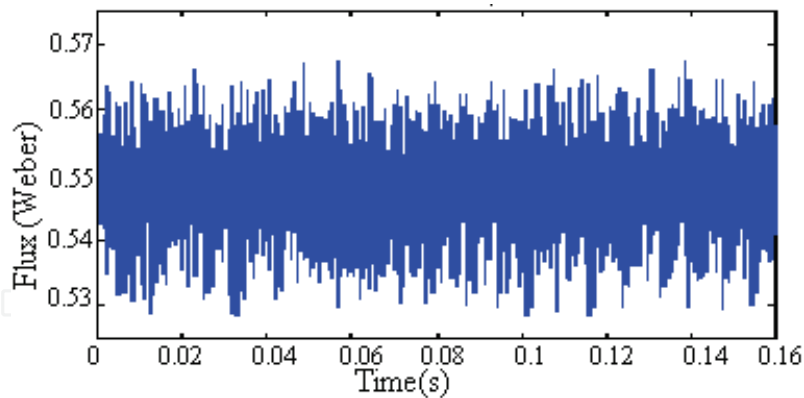

Fig. 21. HDTC Line current of phase-a

Fig. 22. HDTC Flux response

The responses showed that the torque pulsation is also high and line currents are full of switching harmonics as compared to the FOC algorithm. In addition the flux and speed are also not free of ripple which result in machine vibration and acoustic noise.

4. Algorithm 3: Space Vector Modulation Direct Torque Control (SVMDTC)

In this method, a mathematical model of PMSM and space vector modulation of inverter are used to carry out system algorithm. Thus, instead of switching table and hysteresis controller a space voltage modulation vectors depending on the flux positions are used to compensate for errors in flux and torque (Dariusz et al, 2002; Tang et al., 2004). One of the SVM-DTC block diagrams is shown in Fig. 23 (Dariusz et al., 2002).
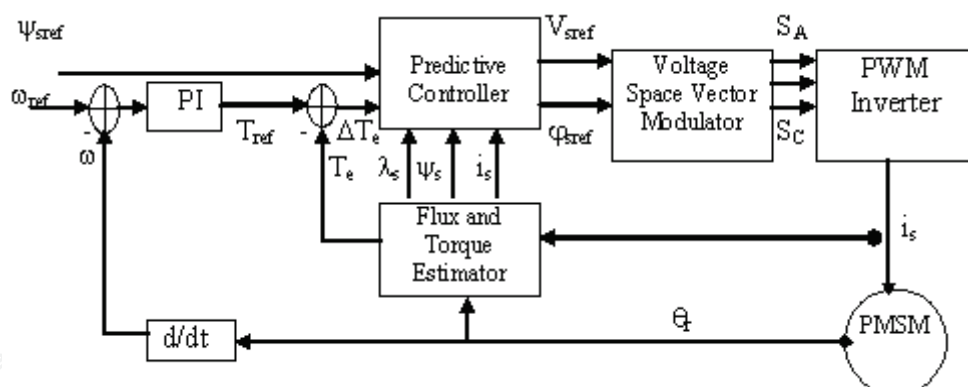

Fig. 23. Direct Torque Control SV-Modulation

In Fig. 23, the torque error signal ΔT_e and reference amplitude of the stator flux Ψ_{sref} are delivered to predictive controller, which also uses information about the amplitude and position of the actual stator flux vector and measured stator current vector. The predictive controller determines the stator voltage command vector in polar co-ordinates $V_{sref} = |V_{sref}| \angle \varphi_{sref}$ for space vector modulator (SVM) which finally generates the pulses S_A, S_B and S_C to control the PWM inverter.

Referring to Eq. (7), the electromagnetic torque produced by the motor is given by:

$$T_e = \frac{3}{2} P \frac{|\psi_s|}{L_d L_q} \left[\psi_F L_q \sin\delta + \tfrac{1}{2}|\psi_s|(L_{sd} - L_{sq})\sin 2\delta \right] \qquad (17)$$

From this equation, it can be seen that for constant stator flux amplitude and flux produced by the permanent magnet, the electromagnetic torque can be changed by control of the torque angle. The torque angle δ can be changed by changing position of the stator flux vector with respect to the PM vector using the actual voltage vector supplied by the PWM inverter (Dariusz, 2002). The flux and torque values can be calculated as in Section 3.1 or may be estimated as in Section 3.3. The internal flux calculator is shown in Fig. 24.
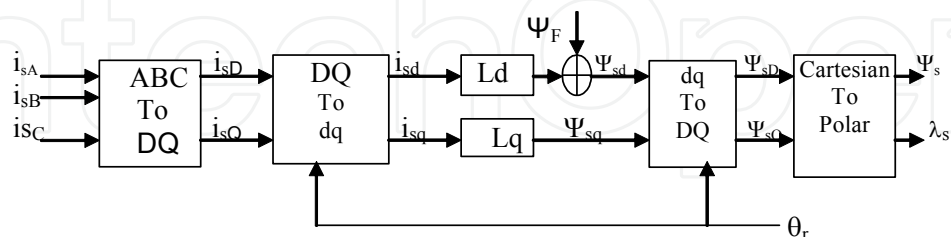

Fig. 24. Flux Estimator Block Diagram

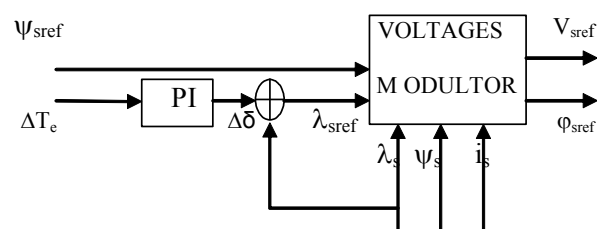The internal structure of the predictive controller is in Fig. 25.

Fig. 25. Predictive Controller

Sampled torque error ΔT_e and reference stator flux amplitude Ψ_{sref} are delivered to the predictive controller. The error in the torque is passed to PI controller to generate the increment in the load angle $\Delta\delta$ required to minimize the instantaneous error between reference torque and actual torque value. The reference values of the stator voltage vector are calculated as:

$$V_{sref} = \sqrt{V_{sD\_ref}{}^2 + V_{sQ\_ref}{}^2} \quad and \quad \varphi_{sref} = \tan^{-1}\frac{V_{sQ\_ref}}{V_{sD\_ref}} \tag{18}$$

Where:

$$V_{sD\_ref} = \frac{\psi_{sref}\cos(\lambda_s + \Delta\delta) - \psi_s\cos\lambda_s}{T_s} + R_s i_{sD}. \tag{19}$$

$$V_{sQ\_ref} = \frac{\psi_{sref}\sin(\lambda_s + \Delta\delta) - \psi_s\sin\lambda_s}{T_s} + R_s i_{sQ}. \tag{20}$$

Where, T_s is the sampling period.

For constant flux operation region, the reference value of stator flux amplitude is equal to the flux amplitude produced by the permanent magnet. So, normally the reference value of the stator flux is considered to be equal to the permanent magnet flux.

4.1 Implementation of SVMDTC

The described system in Fig. 23 has been implemented in Matlab/Simulink, with the same data and loading condition as in HDTC with PI controllers setting as:

Predictive Controller: Ki=0.03, Kp=1 Speed Controller: Ki= 1 Kp=0.04.

The simulation results are shown in Fig. 26 to Fig. 29. As evidence from the figures, the SVM-DTC guarantee lower current pulsation, smooth speed as well as lower torque pulsation. This is mainly due to the fact that the inverter switching in SVM-DTC is uni-polar compared to that of FOC & HDTC (see Fig. 10, Fig. 20 and Fig. 28), in addition the application of SVM reduces switching stress by avoiding direct transition from +Vdc to – Vdc and thus avoiding instantaneous current reversal in dc link. However, the dynamic response in Fig. 9, Fig. 19, and Fig. 27 show that HDTC has faster response compared to the SVM-DTC and FOC.
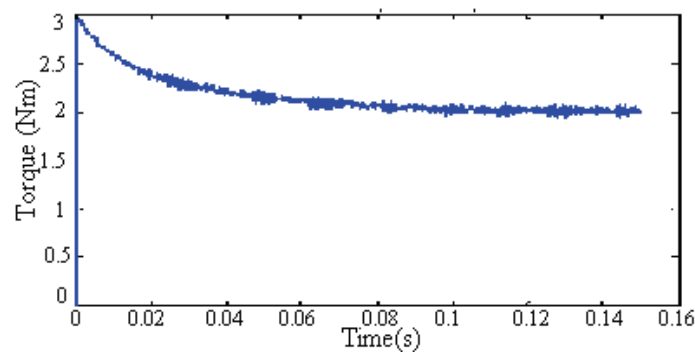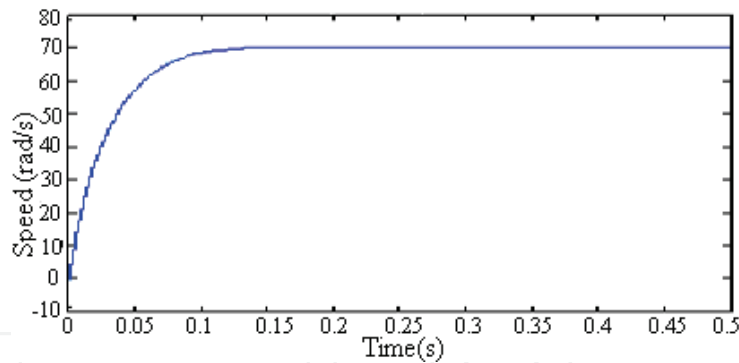

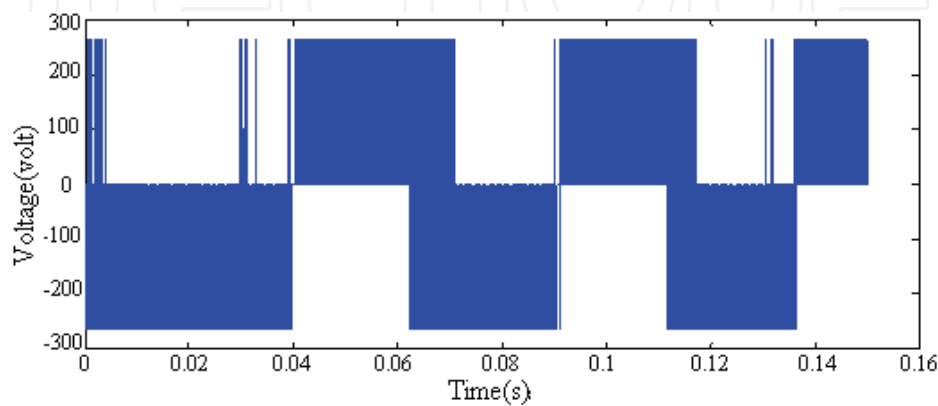Fig. 26. SVMDTC torque response

Fig. 27. SVMDTC rotor speed response

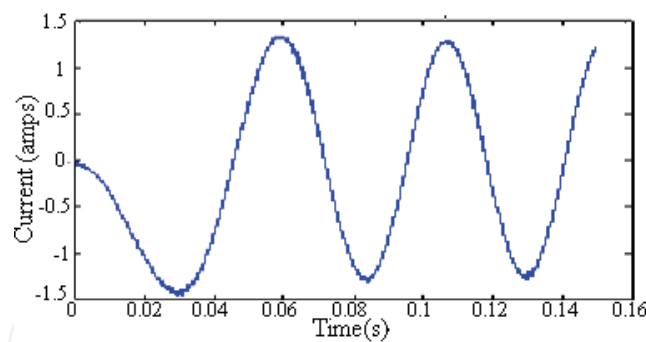Fig. 28. SVMDTC Line voltage (V_{ab}) waveform

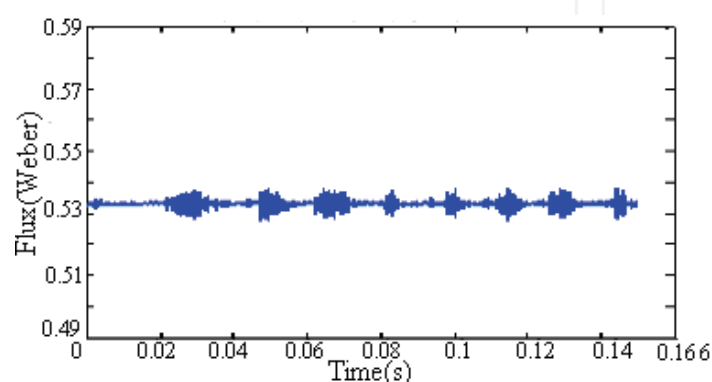Fig. 29. SVMDTC Line current response of phase a

Fig. 30. Stator flux response.

5. High Performance Direct Torque Control Algorithm (HP-DTC)

In this section, a new direct torque algorithm for IPMSM to improve the performance of hysteresis direct torque control is described. The algorithm uses the output of two hysteresis controllers used in the traditional HDTC to determine two adjacent active vectors. The algorithm also uses the magnitude of the torque error and the stator flux linkage position to select the switching time required for the two selected vectors. The selection of the switching time utilizes suggested table structure which, reduce the complexity of calculation. Two Matlab/Simulink models, one for the HDTC, and the other for the proposed model are programmed to test the performance of the proposed algorithm. The simulation results of the proposed algorithm show adequate dynamic torque performance and considerable torque ripples reduction as well as lower flux ripples, lower harmonic current and lower EMI noise reduction as compared to HDTC. Only one PI controller, two hysteresis controllers, current sensors and speed sensor as well as initial rotor position and built-in counters microcontroller are required to achieve this algorithm (Adam & Gulez, 2009).

5.1 Flux and torque bands limitations

In HDTC the motor torque control is achieved through two hysteresis controllers, one for stator flux magnitude error control and the other for torque error control. The selection of one active switching vector depends on the sign of these two errors without inspections of their magnitude values with respect to the sampling time and level of the applied stator voltage. In this section, short analysis concerning this issue will be discussed.

5.1.1 Flux band

Consider the motor stator voltage equation in space vector frame below:.

$$V_s = R_s i_s + \frac{d\Psi_s}{dt} \tag{21}$$

Equation (21) can be written as:

$$dt = \frac{d\Psi_s}{V_s - R_s i_s} \tag{22}$$

For small given flux band $\Delta\Psi_s^o$, the required fractional time to reach the limit of this value from some reference flux Ψ^* is given by:

$$\Delta t = \frac{\left|\Delta\Psi_s^0\right|}{\left|V_s - R_s i_s\right|} \tag{23}$$

And if the voltage drop in stator resistance is ignored, then the maximum time for the stator flux to remain within the selected band starting from the reference value is given as:

$$\Delta t_{\max} = \frac{\left|\Delta\Psi_s^0\right|}{\left|V_s\right|} = \frac{\left|\Delta\Psi_s^0\right|}{\left|2/3\ V_{dc}\right|} \tag{24}$$

Thus if the selected sampling time Ts is large than Δt_{max}, then the stator flux linkage no longer remains within the selected band causing higher flux and torque ripples.

According to (24) if the average voltage supplying the motor is reduced to follow the magnitude of the flux linkage error, the problem can be solved, i.e. the required voltage level to remain within the selected band is:

$$V_{level} = \frac{\Delta t_{\max}}{T_s} V_{kk} \tag{25}$$

Where V_{kk} is the applied active vectors

Thus, by controlling the level of the applied voltage, the control of the flux error to remain within the selected band can be achieved. For transient states, $\Delta\Psi_s$ is most properly large which, requires large voltage level to be applied in order to bring the machine into steady state as quickly as possible.

5.1.2 Torque band

The maximum time Δt_{torque} for the torque ripples to remain within selected hysteresis band can be estimated as:

$$\Delta t_{torque} = \frac{\left|\Delta T^0\right|}{\left|Te_{ref}\right|} * t^0 \tag{26}$$

Where, ΔT^0; is the selected torque band

Te_{ref} ; is the reference electromagnetic torque

t^0; is the time required to accelerate the motor from standstill to some reference torque Te_{ref}.
The minimum of the values given in (24) and (26) can be considered as the maximum switching time to achieve both flux and torque bands requirement. However, when the torque ripples is the only matter of concern, as considered in this work, may be enough to consider the maximum time as suggested by (26).

Now due to flux change by $\Delta\Psi_s$, the load angle δ will change by $\Delta\delta$ as shown in Fig. 31. Under dynamic state, this change is normally small and can be approximated as:

$$\Delta\delta \approx \sin^{-1}\frac{\Delta\Psi_s}{|\Psi_s|} \approx \frac{\Delta\Psi_s}{|\Psi_s|} \qquad (27)$$
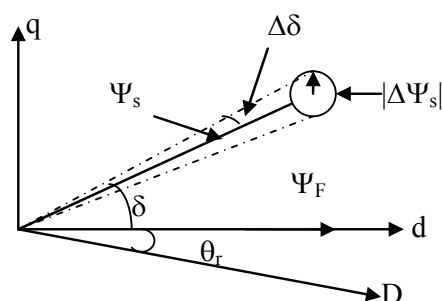

Fig. 31. Stator flux linkage variation under dynamic state

The corresponding change in torque due to change $\Delta\Psi_s$ can be obtained by differentiation of torque equation with respect to δ. Torque equation can be rewritten as:

$$T_e = \frac{3}{4}P\frac{|\Psi_s|}{L_{sd}L_{sq}}\Big[2\Psi_F L_{sq}\sin\delta - |\Psi_s|(L_{sq}-L_{sd})\sin 2\delta\Big] \qquad (28)$$

Where, then

$$\Delta T = \frac{\partial T_e}{\partial \delta}\cdot\Delta\delta \approx \frac{\partial T_e}{\partial \delta}\cdot\frac{\Delta\psi_s}{|\Psi_s|} \qquad (29)$$

Substitute (24) in (29) and evaluate to obtain:

$$\Delta T = \frac{3}{2}P\frac{|V_s|\Delta t}{L_{sd}L_{sq}}\Big[\Psi_F L_{sq}\cos\delta - |\Psi_s|(L_{sq}-L_{sd})\cos 2\delta\Big] \qquad (30)$$

Where, $\Delta t = minimum\ (\Delta t_{max}, \Delta t_{torque})$

Equation (30) suggests that ΔT can also be controlled by controlling the level of V_s. Thus both ΔT and $\Delta\Psi_s$ can be controlled to minimum when the average stator voltage level is controlled to follow the magnitude of ΔT.

5.2 The HP-DTC Algorithm

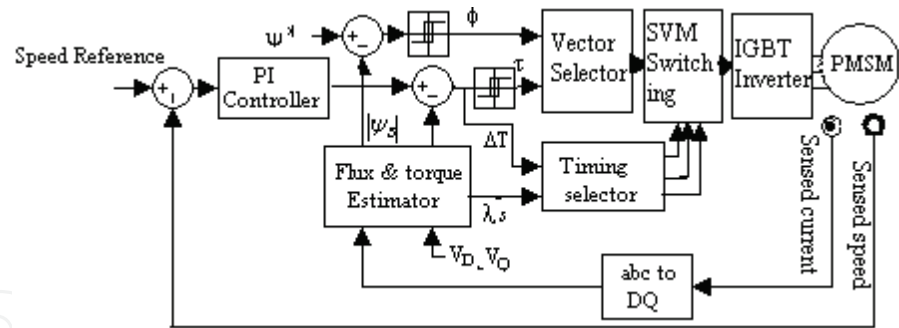The basic structure of the proposed algorithm is shown in Fig. 32.

Fig. 32. The HPDTC system of PMSM

5.2.1 Vector selector
In Fig.32 the vector selector block contains algorithm to select two consecutive active vectors V_{k1}, and V_{k2} depending on the output of the hysteresis controllers of the flux error and the torque error; ϕ and τ respectively as well as flux sector number; n. The vector selection table is shown in Table 4., while vectors position and flux sectors is as shown in Fig.15

ϕ	τ	V_{k1}	V_{k2}
1	1	n+1	n+2
1	0	n-1	n-2
0	1	n+2	n+1
0	0	n-2	n-1

Table 4. Active vectors selection table

In the above table

if $V_k > 6$ then $V_k = V_k - 6$

if $V_k < 1$ then $V_k = V_k + 6$

5.2.2 Flux and torque estimator
In Fig. 32 the torque and flux estimator utilizes equation (21) to estimate flux and torque values at m sampling period as follows:

$$\psi_D(m) = \psi_D(m-1) + (V_D(m-1) - R_s i_D)T_s \tag{31}$$

$$\psi_Q(m) = \psi_Q(m-1) + (V_Q(m-1) - R_s i_Q)T_s \tag{32}$$

$$|\psi_s| = \sqrt{\psi_D^2 + \psi_Q^2} \tag{33}$$

$$\lambda_s = Tan^{-1}\frac{\psi_Q}{\psi_D} \tag{34}$$

Where; the stationary D-Q axis voltage and current components are calculated as follows:

$$V_D(m-1) = (V_{Dk1}t_{k1} + V_{Dk2}t_{k2})/Ts \tag{35}$$

$$V_Q(m-1) = (V_{Qk1}t_{k1} + V_{Qk2}t_{k2}) / Ts \tag{36}$$

$$i_D = (i_D(m-1) + i_D(m)) / 2 \tag{37}$$

$$i_Q = (i_Q(m-1) + i_Q(m)) / 2 \tag{38}$$

The torque value can be calculated using estimated flux values as:

$$T_e = \frac{3}{2}P(\Psi_D(m)i_Q(m) - \Psi_Q(m)i_D(m)) \tag{39}$$

5.2.3 The timing selector structure

In Fig. 32 the timing selector block contains algorithm to select the timing period pairs of vectors V_{k1} and V_{k2}. The selection of timing pairs depends on two axes, one is the required voltage level and the other is the reflected flux position in the sector contained between V_{k1} and V_{k2}. The reflected flux position is given by:

$$\rho_s = \lambda_s \bmod 60 - \pi / 6 \tag{40}$$

Where λ_s; is the stator flux linkage position in D-Q stationary reference frame.

Fig. 34 shows the proposed timing table. In this figure, the angle between the two vectors V_{k1} and V_{k2} which is 60^0, is divided into 5 equal sections ρ_{-2}, ρ_{-1}, ρ_0, ρ_{+1}, and ρ_{+2}. The required voltage level is also divided into 5 levels.

The time pairs (t_{k1}, t_{k2}), expressed as points, (out of 20 points presenting the sampling period) define the timing periods of V_{k1} and V_{k2} respectively. The remaining time points, ($t_0=20-t_{k1}-t_{k2}$), is equally divided between zero vectors V_0 and V_7.
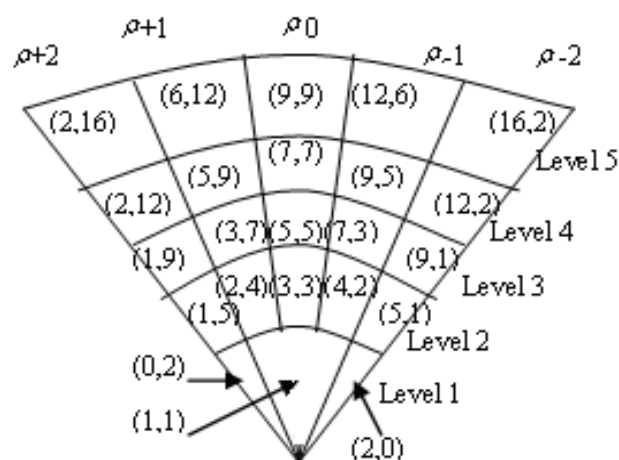

Fig. 34. Timing diagram for the suggested algorithm

The time structure shown in Fig.34 has the advantage of avoiding the complex mathematical expressions used to calculate t_{k1} and t_{k2}, as the case in space vector modulation used by (Dariusz, 2002) and (Tan, 2004). In addition, it is more convenient to be programmed and executed through the counter which controls the period t_{k1}, t_{k2} and t_0. The flow chart of the algorithm is shown in Fig. 35.
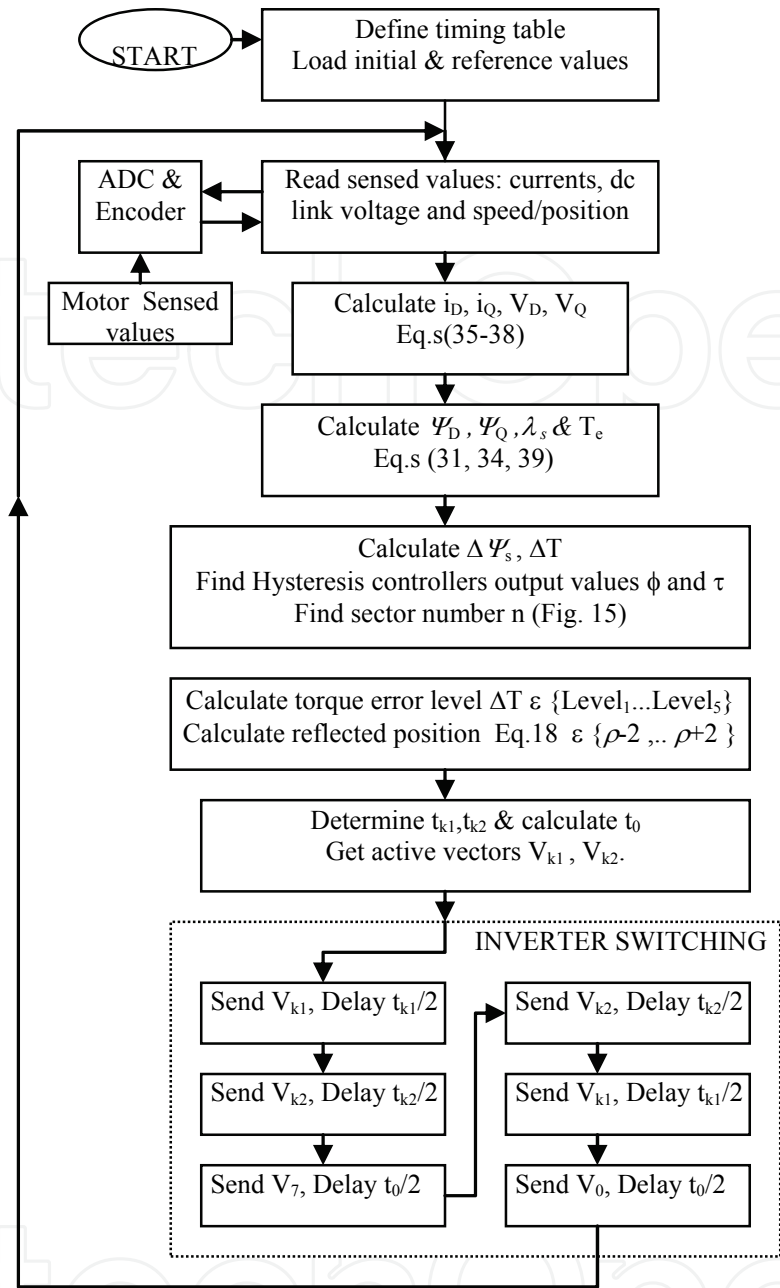
Fig. 35. A Flow chart of the proposed algorithm

5.3 Simulation and results

To examine the performance of the proposed DTC algorithm, two Matlab/Simulink models, one for HDTC and the other for the HPDTC were programmed. The motor parameters are shown in table 2. The inverter used in simulation is IGBT inverter with the following setting: IGBT/Diode

Snubber Rs, Cs = (1e-3ohm,10e-6F)

Ron=1e-3ohm

Forward voltage (V_f Device,V_f Diode)= (0.6, 0.6)

$T_f(s), T_t(s) = $ (1e-6, 2e-6)

DC link voltage= +132 to -132.

The simulation results with 100µs sampling time for the two algorithms under the same operating conditions are shown in Fig. 36 -to- Fig. 41. The torque dynamic response is simulated with open speed loop, while the steady state performance is simulated with closed speed loop, 70rad/s as reference speed, and 2 Nm as load torque.

5.3.1 Torque dynamic response

The torque dynamic response with HDTC and the HPDTC are shown in Fig.36-a and Fig.36-b respectively. The reference torque for both algorithms is changed from +2.0 to -2.0 and then to 3.0 Nm. As shown in the figures, the dynamic response with the proposed algorithm is adequately follows the reference torque with lower torque ripples. In the other hand, the torque response with the proposed algorithm shows fast response as the HDTC response.
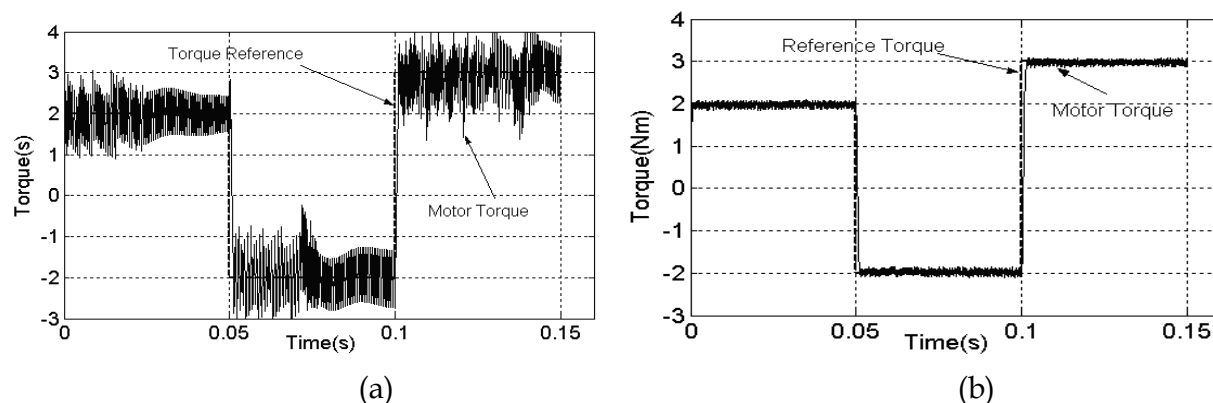

Fig. 36. Motor dynamic torque with opened speed loop: (a) HDTC (b) HP-DTC

Fig. 37 demonstrates the idea of maximum time to remain within the proposed torque band as suggested by equation (26). According to the shown simulated values, the time required to accelerate the motor to 2 Nm is $\approx$ 0.8ms, so if the required limit torque ripple is not to exceed 0.1 Nm, as suggested in this work, then, the maximum switching period according to Eq. (26) is $\approx$0.05ms which is less than the sampling period (Ts=0.1 ms).
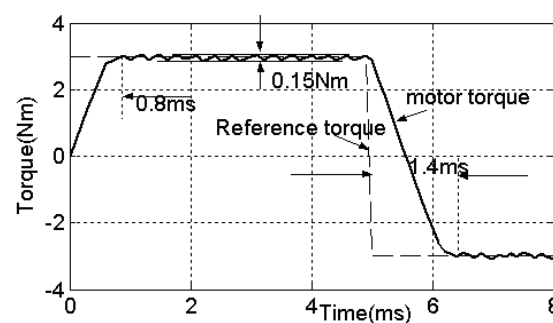

Fig. 37. Torque ripples and motor accelerating time

Although the torque ripple is brought under control, the flux ripples still high as shown in Fig. 38 which, is mainly due to control of the voltage level according to the magnitude of torque error only.
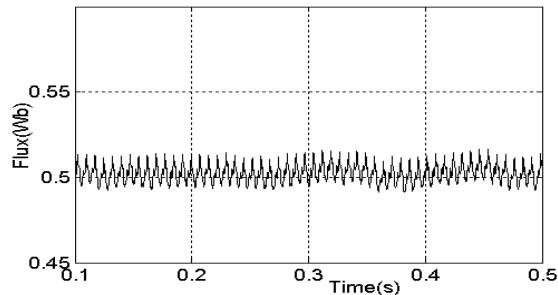
Fig. 38. Flux response when only the torque error magnitude is used to approximate the required voltage level

5.3.2 Motor steady state performance

The motor performance results under steady state are shown in Fig. 39 -to- Fig. 41. Fig. 39-a and Fig. 39-b, show the phase currents of the motor windings under HDTC and the HPDTC respectively, observe the change of the waveform under the proposed method, it is clear that the phase currents approach sinusoidal waveform with almost free of current pulses appear in Fig. 39-a. Better waveform can be obtained by increasing the partition of the timing structure, however, when smoother waveform is not necessary, suitable division as the one shown in Fig. 34 may be enough.
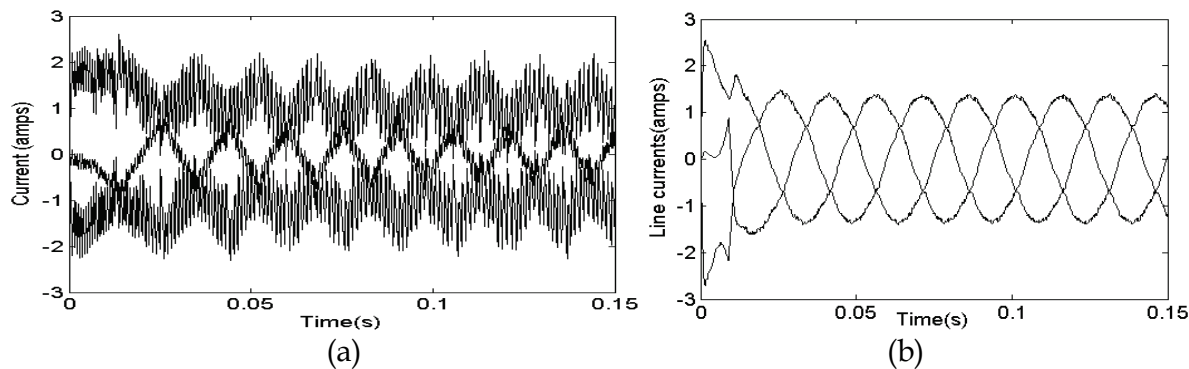

Fig. 39. Motor line currents: (a) HDTC (b) HPDTC

The torque response in Fig. 40 shows considerable reduction in torque ripples from 3.2Nm (max. -to- max.) down to less than 0.15 Nm when the new method HP-DTC is used, which in turn, will result in reduced motor mechanical vibration and acoustic noise, this reduction also reflected in smoother speed response as shown in Fig. 41
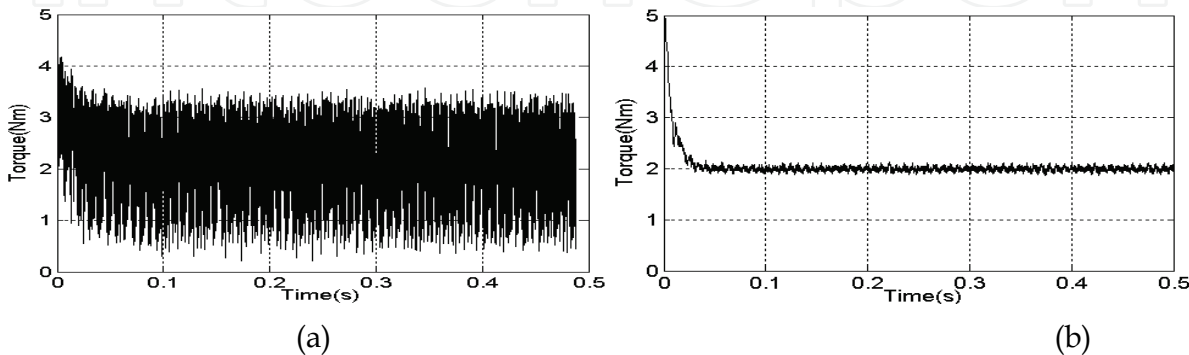

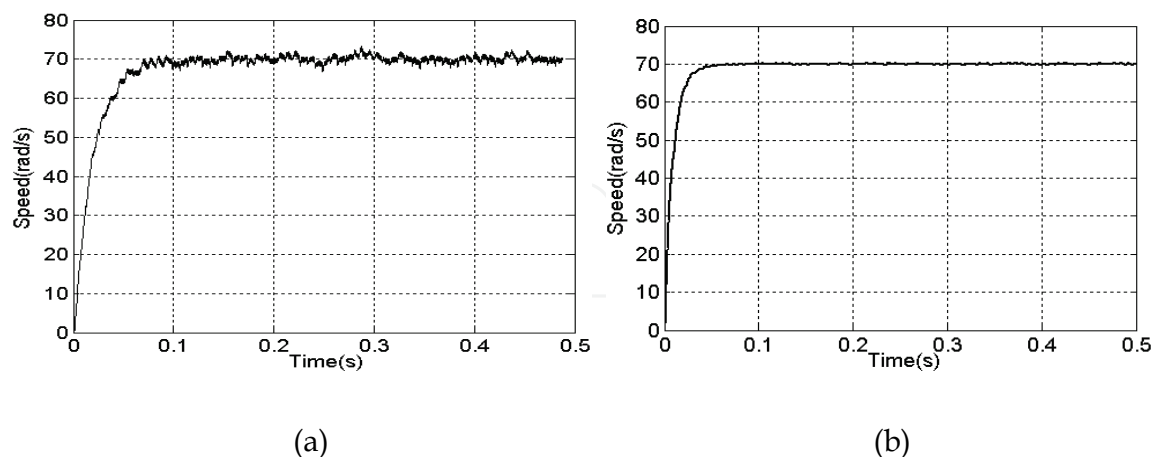Fig. 40. Motor steady state torque response: (a) HDTC (b) HPDTC

(a)   (b)

Fig. 41. Rotor speed response: (a) HDTC (b) HPDTC

6. Torque ripple and noise in PMSM algorithm

One of the major disadvantages of the PMSM drive is torque ripple that leads to mechanical vibration and acoustic noise. The sensitivity of torque ripple depends on the application. If the machine is used in a pump system, the torque ripple is of no importance. In other applications, the amount of torque ripple is critical. For example, the quality of the surface finish of a metal working machine is directly dependent on the smoothness of the delivered torque (Jahns and Soong, 1996). Also in electrical or hybrid vehicle application, torque ripple could result in vibration or noise producing source which in the worst case could affect the active parts in the vehicle.

The different sources of torque ripples, harmoinc currents and noises in permanent magnet machines can be abstracted in the following (Holtz and Springob 1996,1998):

- Distortion of the stator flux linkage distribution
- Stator slotting effects and cogging
- Stator current offsets and scaling errors
- Unbalanced magnetization
- Inverter switching and EMI noise

However switching harmonics and voltage harmonics supplied by the power inverter constitute the major source of harmonics in PMSM. In this section, the reduction of torque ripple and harmonics generated due to inverter switching in PMSM control algorithms using passive and active filter topology will be investigated.

Method1: Compound passive filter topology
6.1 The proposed passive filter topology

Fig. 42 shows a block diagram of basic structure of the proposed filter topology (Gulez et al., 2007) with PMSM drive control system. It consists of compound dissipative filter cascaded by RLC low pass filter. The compound filter has two tuning frequency points, one at inverter switching frequency and the other at some average selected frequency.
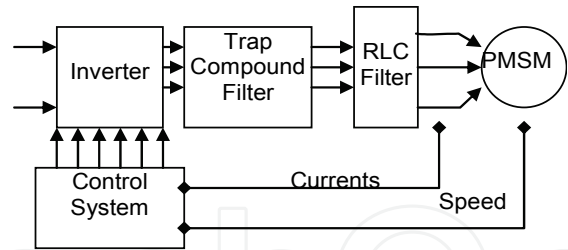
Fig. 42. Block diagram of the proposed filter topology with PMSM drive system

6.1.1 The compound trap filter

Fig. 43 shows the suggested compound trap filter. It consists of main three passes, one is low frequency pass branch through R_2 and L_2, another is the high frequency pass through C_2 and R_1 and the other is the average frequency pass through C_1, L_1 and R_1 to the earth.
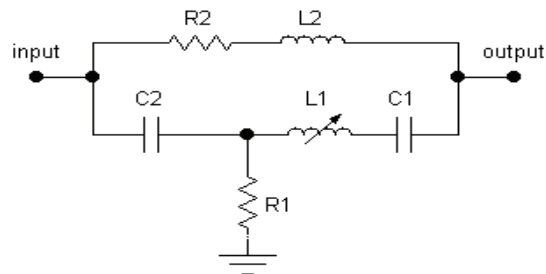

Fig. 43. The suggested compound trap filter

For some operating frequency ω_o, the component of the low pass branch constitutes low impedance path while at the same time shows high impedance for the high frequency component, which forces the high frequency to pass through C_2 to the earth. Some of the average frequency components will find their way through the low pass branch. These frequencies will be absorbed by tuning resonance of branch L_1-C_1 to some selected average frequency such that.

$$\omega_o < \omega_{av} < \omega_{sw}$$

Where
ω_o ; is the operating frequency

$\omega_{av} = 1 / \sqrt{L_1 C_1}$: is the selected average frequency

ω_{sw}: is inverter switching frequency calculated as $1/(2T_s)$; T_s being the sampling period
The behavior of the Compound Trap filter can be explained by studying the behavior of the impedances constitutes the Π equivalent circuit of the Compound Trap filter shown in Fig. 44.
In Fig. 44 the impedances Z_1, Z_2 and Z_3 can be expressed as:

$$Z_1 = \frac{\omega L_1 - 1 / \omega c_1}{\omega R_1 C_2} + j(\omega L_1 - \frac{1}{\omega C_1} - \frac{1}{\omega C_2}) \tag{41}$$
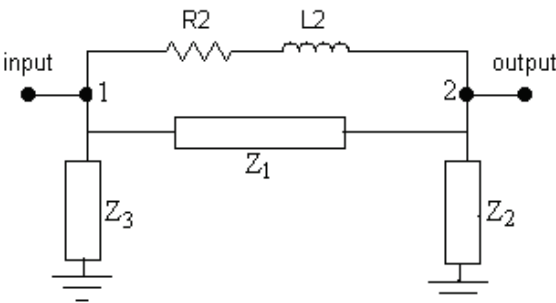
Fig. 44. Equivalent Π circuit of the compound trap filter.

$$Z_2 = R_1 - R_1 C_2 \omega(\omega L_1 - \frac{1}{\omega C_1}) + j(\omega L_1 - \frac{1}{\omega C_1}) \tag{42}$$

$$Z_3 = R_1 - \frac{R_1}{\omega^2 L_1 C_2 - C_2 / C_1} - j\frac{1}{\omega C2} \tag{43}$$

Figures 45, 46 and 47 show the frequency-magnitude characteristics of the impedances Z_2, Z_3 and Z_{12} respectively. Z_{12} is the equivalent impedance value between point 1 and 2 as shown in Fig. 44.
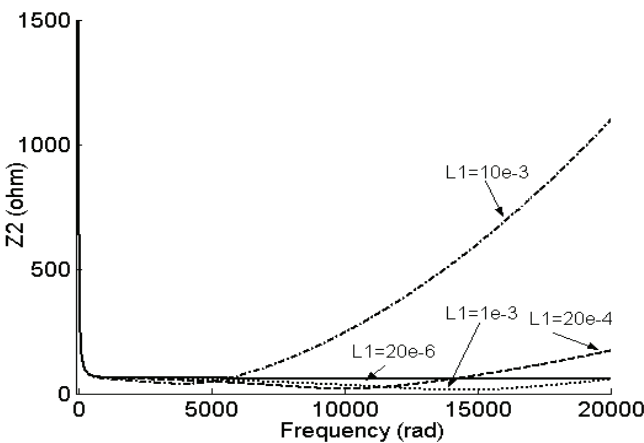

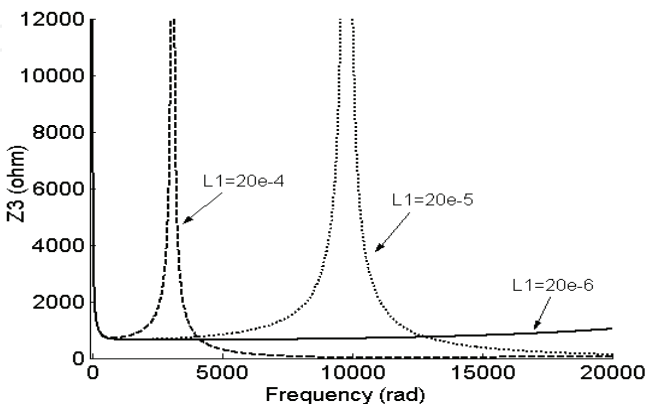Fig. 45. Z_2 characteristics at C1=52.0e-6F and different L_1 values.

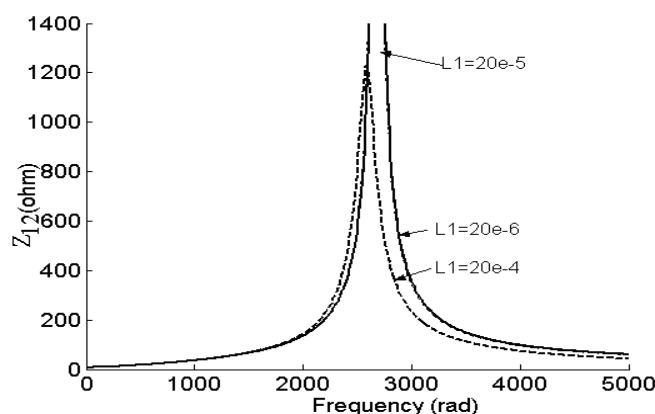Fig. 46. Z_3 characteristics at C1=52.0e-6F and different L_1 values.

Fig. 47. Z_{12} characteristics at C1=52.0e-6F and different L_1 values.

As can be inferred from Equations (41 to 43) and Figures (Fig. 46 to Fig. 47) it is evidence that both Z_2 and Z_3 show capacitive behavior at small values of L_1. So if the value of L_1 is kept small (L1 < 1e-5 H), the tuning of high frequency current components is ensured through the compound trap filter.

In the other hand the characteristics of Z_{12} shown in Fig. 47 demonstrates that at average frequencies the impedance of Z_{12} is high while at low and high frequencies the impedance is low thus Z_{12} constitute band stop filter to the average frequency current components. The magnitude of Z_{12} can effectively be changed by changing the value of L1 at constant C1, while the range of the average frequencies can effectively be changed by changing the value of C1 at constant L1. Thus through proper tuning of L1 and C1 the desired average frequency range can be selected.

6.1.2 RLC filter

Fig. 48 shows the suggested RLC filter, which play main role in reducing the high *dv/dt* of line to line voltages at motor terminals. The transfer function of this circuit is given by:

$$\frac{V_0}{V_i} = \frac{R_3 C_3 s + 1}{C_3 L_3 s^2 + (r_3 + R_3) C_3 s + 1} \tag{44}$$

To obtain over damping response, the filter resistances are selected such that:

$$(R_3 + r_3) > \sqrt{\frac{4L_3}{C_3}} \tag{45}$$

With cutoff frequency ω_c is given by:

$$\omega_c = 1 / \sqrt{L_3 C_3} \tag{46}$$

To reduce ohmic losses the series resistance r_3 is normally of small value, while the shunt resistance R_3 is selected high enough to limit the currents drawn by the filter. This current can be expressed as:

$$i_{CR3} = \frac{z_{PMSM}}{z_{PMSM} + \sqrt{R_3^2 + (1 / sC_3)^2}} i_{in} \tag{47}$$

Where, Z_{PMSM} is PMSM motor input impedance.

At the selected cutoff frequency, this current should be large compared to i_{motor} drawn by the motor; while at operating frequency this current should be very small compared to i_{motor}. Another point in selection of the RLC parameters is that, the filter inductors are essentially shorted at line frequency while the capacitors are open circuit and for EMI noise frequencies, the inductors are essentially open circuit while the capacitors are essentially shorted, thus considerable amount of EMI noises will pass through the filter resistors to the earth and cause frequency dependent voltage drop across the series branch of the filter which, in turn, helps in smoothing of the voltage waveform supplying the motor.
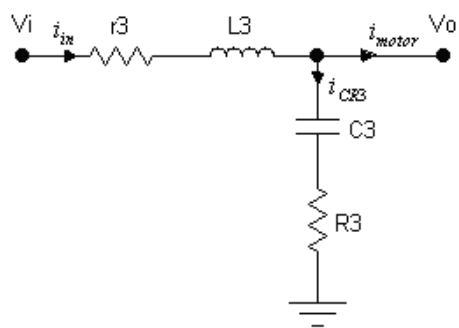

Fig. 48. RLC filter cascaded to the trap compound filter

To evaluate the performance of the suggested passive filter topology, it was applied to HDTC algorithms under MatLab simulation. The following subsections show the results of the simulations.

6.1.3 Torque ripples and noise reduction in HDTC using passive filter

Fig. 49 shows the basic structure of HDTC of PMSM with the proposed passive filter topology. The switching table in Fig.49 is the same as that shown in Table 3. In this figure, the switching of the inverter is updated only when the outputs of the hysteresis controllers change states, which result in variable switching frequency and associated large harmonic range and high current ripples.
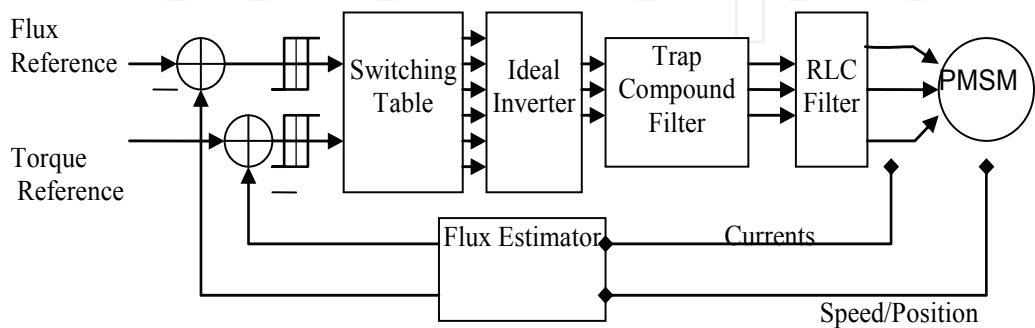

Fig. 49. The basic structure of HDTC of PMSM with the proposed filter topology

6.1.4 Simulations and results

To simulate the performance of the proposed passive filter topology under HDTC Matlab/Simulink was used.

Under base speed operation, the speed control was achieved through PI controller with $K_i = 2.0$ and $K_p = 0.045$. The flux reference is set equal to Ψ_F and hysteresis bands are set to 0.01 for both the torque and flux hysteresis controllers. The motor parameters are shown in Table 2 and the passive filter parameters are in Table 5.

L_1	20µH	L_2	30mH	L_3	30mH
C_1	52µF	C_2	5.1µF	C_3	12.5 µF
R_1	56kΩ	R_2	2.2Ω	R_3	128 Ω
				r_3	2Ω

Table 5. Passive Filter Parameters

The simulation results with 100µs sampling time are shown in Fig. 50 to Fig. 55. Fig. 50-a in particular, shows the motor line voltage V_{ab} without applying the proposed filter topology. When the filter topology is connected, the switching frequency is reduced as depicted in Fig. 50-b compared to the one shown in Fig. 50-a. The line voltages provided to the motor terminals approach sinusoidal waveform, observe the change of the waveform at the output of the compound filter in Fig. 50-c and at the motor terminal in Fig. 50-d. Better waveform as mentioned before can be obtained by increasing the series inductance L_3 and decreasing the resistance r_3.
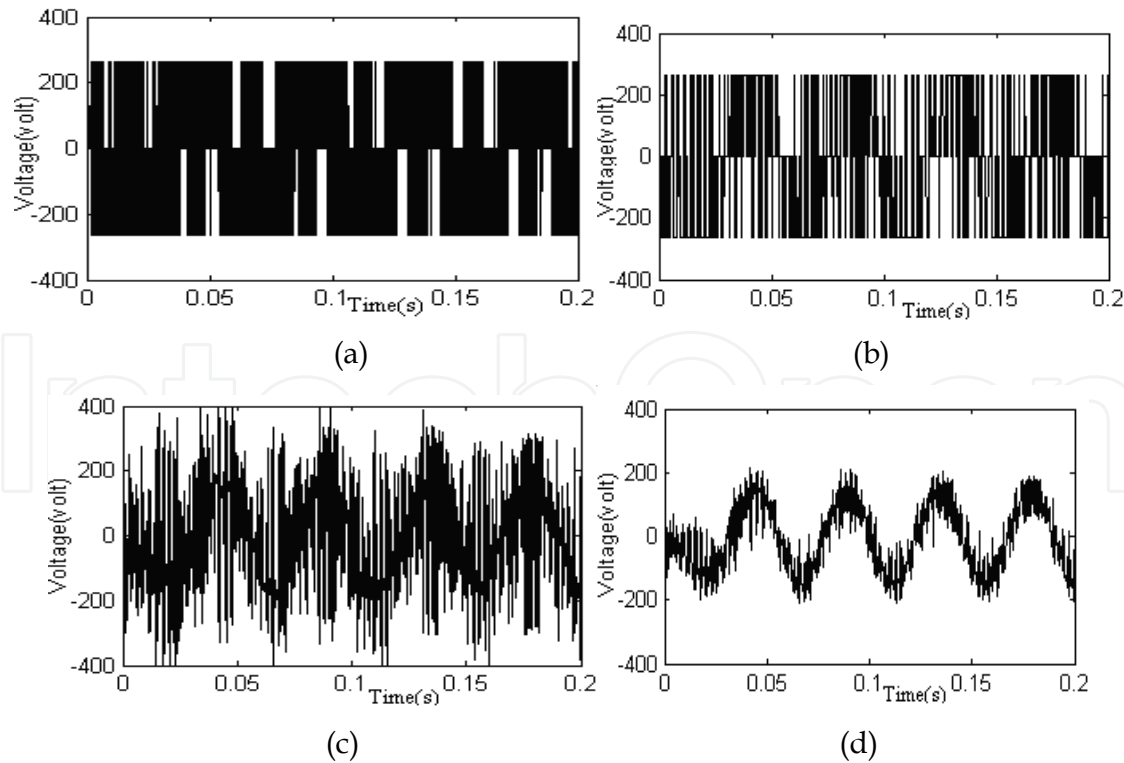

Fig. 50. Motor line voltage (a) before applying the filter topology (b) at inverter terminals after applying the filter topology (c) at the compound Filter output terminals (d) at the motor terminals as output of the RLC filter

The motor performance before and after applying the filter topology are shown in Fig. 51 to Fig. 54. In Fig. 51, the motor line currents show considerable reduction in noise and harmonic components after applying the filter which reflects in smoother current waveform.

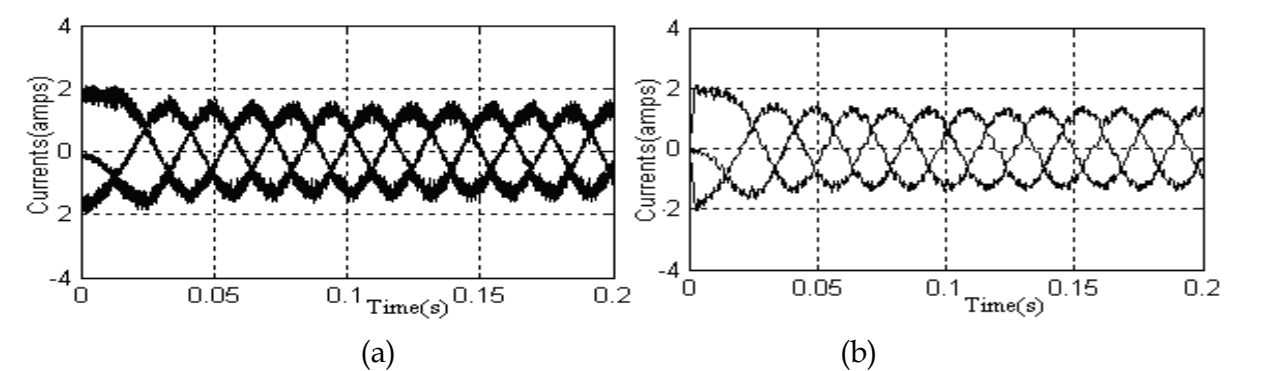(a)   (b)

Fig. 51. Motor line currents: (a) before (b) after applying the filter topology

The torque response in Fig. 52 shows considerable drop in torque ripples from 1.4Nm (ripples to ripples) down to 0.6 Nm after applying the Filter topology, which will result in reduced motor mechanical vibration and acoustic noise. The speed response in Fig. 52, shows slight smoothness after applying the passive filter topology.

The status of the line current harmonics and EMI noise before and after connecting the filter topology are shown in Fig. 53 to Fig. 54.
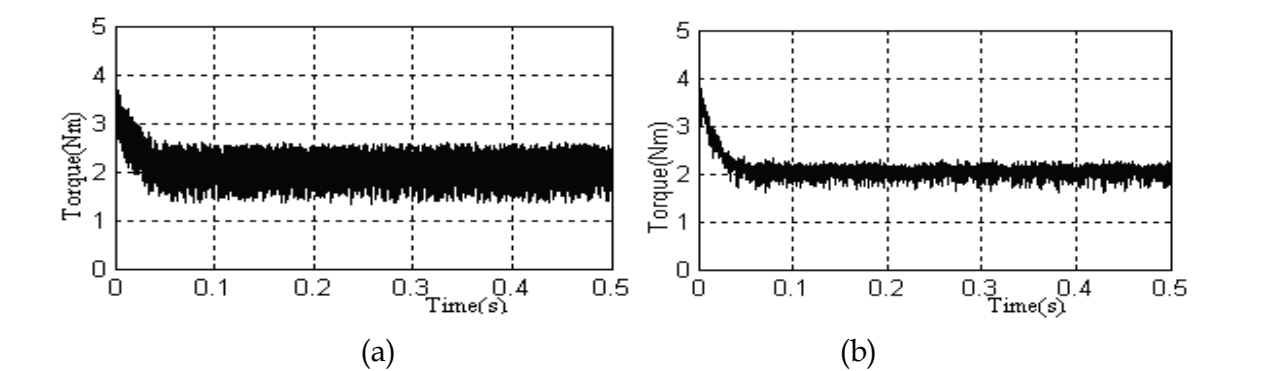

(a)   (b)

Fig. 52. Motor torque: (a) before (b) after applying the filter topology (load torque is 2Nm)

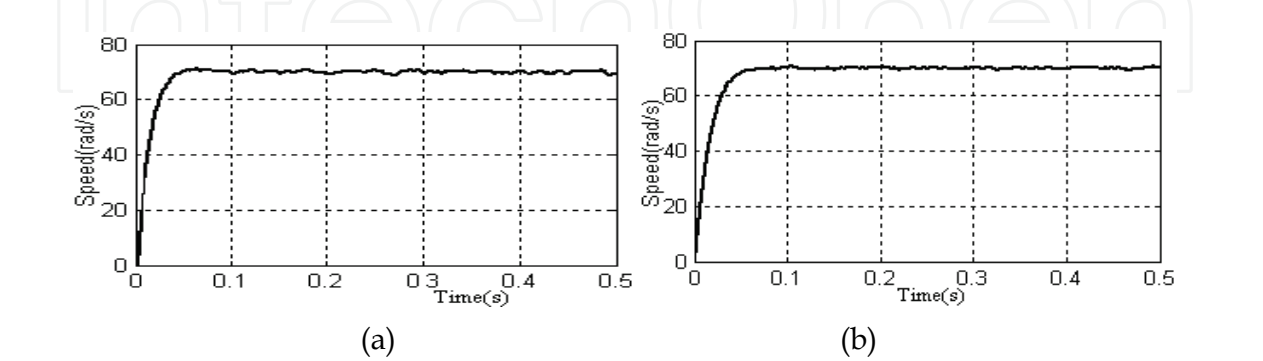(a)   (b)

Fig. 53. Rotor speed: (a) before (b) after applying the filter topology

In Fig. 54-a the spectrum of the line current without connecting the filter shows that harmonics currents with THD of ~3% have widely distributed with a dominant harmonics

concentration in the range around 2 kHz.. After connecting the filter topology, the THD is effectively reduced to less than 1.7% with dominant harmonics concentration in the low frequency range (less than 0.5 kHz.), while the high frequency range is almost free of parasitic harmonics as shown in Fig. 54-b.

(a)   (b)
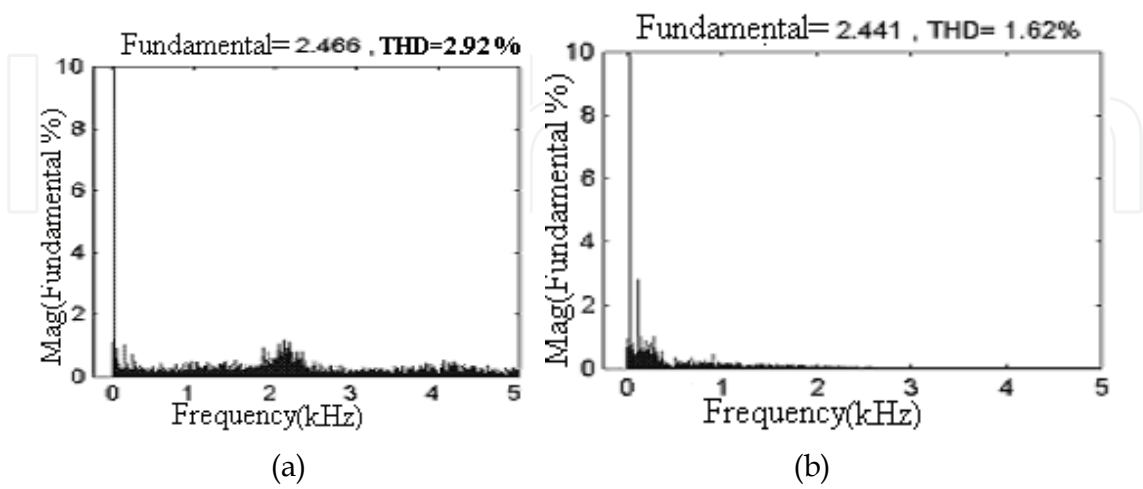
Fig. 54. Phase-a current spectrum: (a) before applying the filter topology (b) after applying the filter topology

The EMI noise level near zero crossing before applying the filter topology in Fig. 55-a shows a noise level of ~ -5dB at operating frequency , ~-10dB at switching frequency (5KHz) and ~-47dB at the most high frequencies (greater than 0.2 MHz.). When the filter is connected, the EMI noise level is damped down to ~-20dB at operating frequency , ~-30dB at switching frequency and ~-67dBs at the most high frequencies as shown in Fig. 55-b.
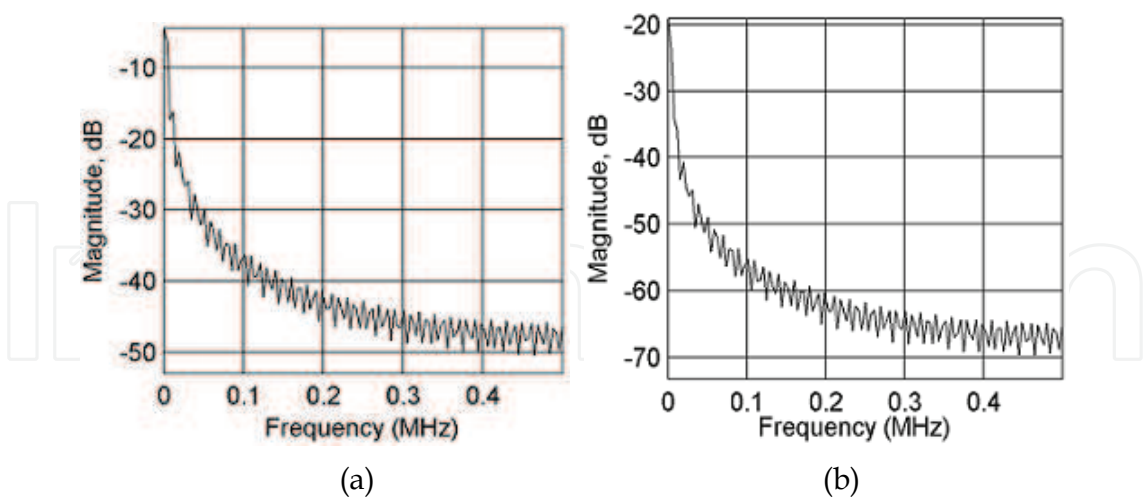

(a)   (b)

Fig. 55. EMI level: (a) before applying the filter topology (b) after applying the filter topology

6.2 Method 2: active filter topology

In this section an active filter topology will be proposed to reduce torque ripples and harmonic noises in PMSM when controlled by FOC or HDTC equipped with hysteresis

controllers. The filter topology consists of IGBT active filter (AF) and two RLC filters, one in the primary circuit and the other in the secondary circuit of a coupling transformer. The AF is characterized by detecting the harmonics in the motor phase voltages and uses hysteresis voltage control method to provide almost sinusoidal voltage to the motor windings.

6.2.1 The proposed active filter topology
When the PMSM is controlled by HDTC, the motor line currents and/or torque are controlled to oscillate within a predefined hysteresis band. Fig. 56, for example, shows typical current waveform and the associated inverter output voltage switching.
In the shown figure the inverter changes state at the end of a sampling period only when the actual line current increases or decrease beyond the hysteresis band which result in high ripple current full of harmonic components.
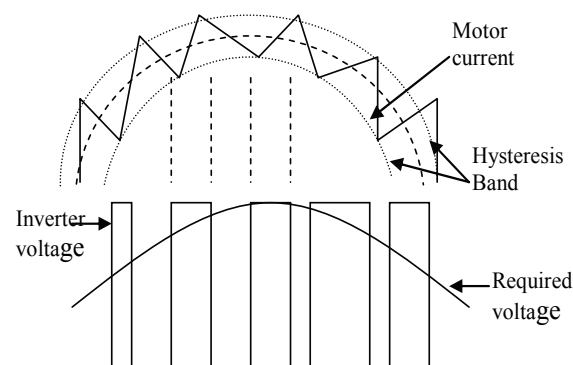

Fig. 56. Current waveform and associated inverter voltage switching equipped with hysteresis controllers

To reduce the severe of these ripples two methods can be mentioned, the first one is to reduce the sampling period which implies very fast switching elements, and the second one is to affect the voltage provided to the motor terminals in such a way to almost follow sinusoidal reference guide. The last method will be adopted here so, active filter topology is used to affect inverter voltage waveform to follow the required signal voltage.
Series active power filters were introduced by the end of the 1980s and operate mainly as a voltage regulator and as a harmonic isolator between the nonlinear load and the utility system (Hugh et al, 2003). Since series active power filter injects a voltage component in series with the supply voltage, they can be regarded as a controlled voltage source. Thus this type of filters is adopted here to compensate the harmonic voltages from the inverter supplying the motor.
Fig. 57 shows a schematic diagram of basic structure of the proposed filter topology; including the active filter, coupling transformer, RLC filters and block diagram of the active filter control circuit
In Fig. 57 V_{sig} is the desired voltage to be injected in order to obtain sinusoidal voltage at motor terminals and V_{AF} is the measured output voltage of the active filter. V_{AF} is subtracted from V_{sig} and passed to hysteresis controller in order to generate the required switching signal to the active filter. The active filter storage capacitor C_F which operates as voltage source should carefully be selected to hold up to the motor line voltage. The smoothing inductance L_F should be large enough to obtain almost sinusoidal voltage at the motor

terminals. The reference sinusoidal voltage V* which should be in phase with the main inverter output voltage V$_{inv}$, is calculated using information of the motor variables.

In the following sections firstly, the operating principle of voltage reference control circuit will be explained then the two other parts will follow.
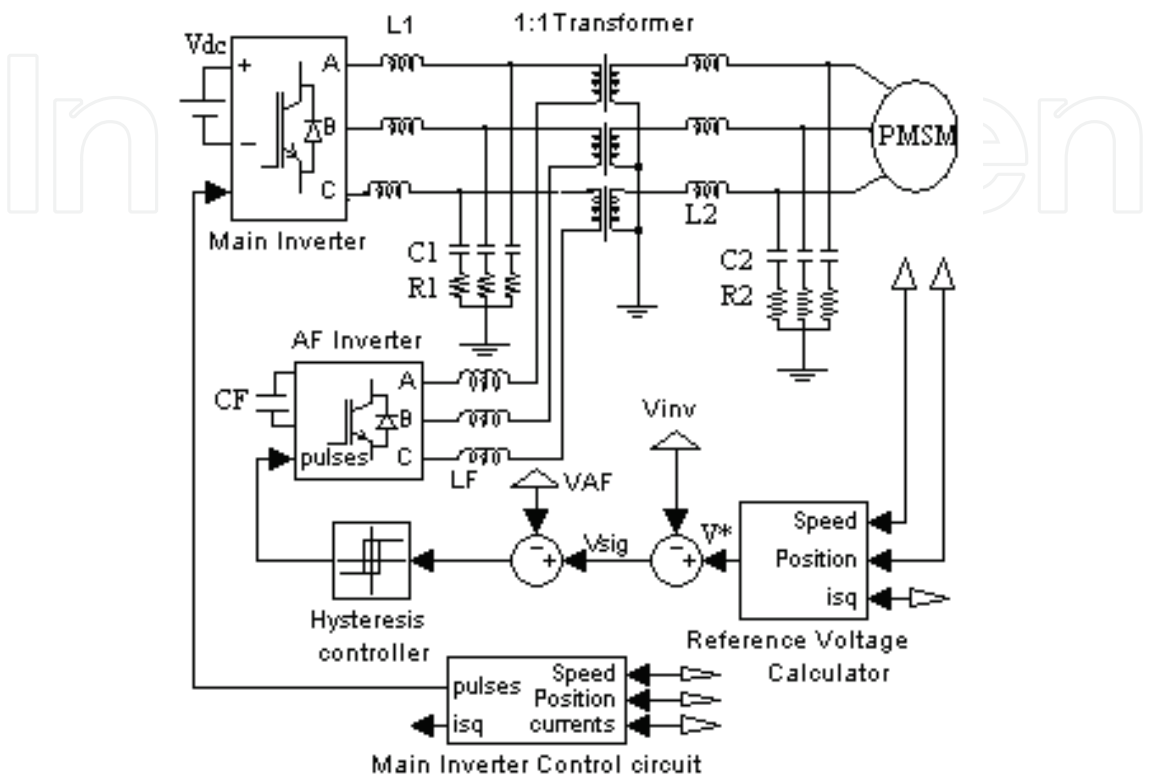

Fig. 57. Basic Structure of the Proposed Filter Topology

6.2.2 Voltage reference signal generator

The effectiveness of the active filter is mainly defined by the algorithm used to generate the reference signals required by the control system. These reference signals must allow current and voltage compensation with minimum time delay. In this study the method used to generate the voltage reference signals is related to FOC algorithm, which use motor model in rotor d-q reference frame and rotor field oriented control principles with monitored rotor position/speed and monitored phase currents. The motor model in this synchronously rotating reference frame is given by:

$$\begin{bmatrix} v_{sd} \\ v_{sq} \end{bmatrix} = \begin{bmatrix} R + pL_{sd} & -\omega_r L_{sq} \\ \omega_r L_{sd} & R + pL_{sq} \end{bmatrix} \begin{bmatrix} i_{sd} \\ i_{sq} \end{bmatrix} + \begin{bmatrix} 0 \\ \omega_r \psi_F \end{bmatrix} \quad (48)$$

$$T_e = \frac{3}{2} P(\psi_F i_{sq} + (L_{sd} - L_{sq}) i_{sd} i_{sq})) \quad (49)$$

Under base speed operation, the speed or torque control can be achieved by forcing the stator current component i_{sd} to be zero while controlling the i_{sq} component to directly proportional to the motor torque T_e as in (50):

$$T_e = \frac{3}{2} P \psi_F i_{sq} \tag{50}$$

The instantaneous q-axis current can be extracted from (50) and hence by setting i_{sd} to zero, the instantaneous d and q axis voltages can be calculated from (48) as:

$$V_{sd} = -\omega_r L_{sq} i_{sq} \tag{51}$$

$$V_{sq} = R i_{sq} + p L_{sq} i_{sq} + \omega_r \psi_F \tag{52}$$

Once the values of d-axis and q-axis voltage components are obtained, Park and Clarke transformation can be used to obtain the reference sinusoidal voltages as:

$$\begin{bmatrix} v_a^* \\ v_b^* \\ v_c^* \end{bmatrix} = K \begin{bmatrix} 1 & 0 \\ -1/2 & \sqrt{3}/2 \\ -1/2 & -\sqrt{3}/2 \end{bmatrix} \begin{bmatrix} \cos\theta & -\sin\theta \\ \sin\theta & \cos\theta \end{bmatrix} \begin{bmatrix} V_{sd} \\ V_{sq} \end{bmatrix} \tag{53}$$

Where, K is the transformation constant and θ is rotor position

6.2.3 Active filter compensation circuit
Fig. 58 shows simplified power circuit of the proposed topology (*the passive RCL filters are not shown*). In this circuit V_{dc} is the voltage of the main inverter circuit, $V_{CF}^{\pm}$ is equivalent compensated voltage source of the active filter. In order to generate the required compensation voltages that follow the voltage signal v_{sig}; *bearing in the mind that the main inverter change switching state only when the line current violates the condition of the hysteresis band and that the capacitor voltage polarity can not change abruptly,* the switches sw₁ and sw₂ are controlled within each consecutive voltage switching of the main inverter to keep the motor winding voltages with acceptable hysteresis band.

The motor line current i_m is controlled within the motor main control circuit with hysteresis current controller to provide the required load torque; therefore, two hysteresis controller systems, one for voltage and the other for current are working independently to supply the motor with almost sinusoidal voltage

In Fig. 58, when switching signal (eg.100) is send to the main inverter, i.e. phase a is active high while phase b and c are active low, then, following the path of the current i_m in Fig.58 the voltage provided to the motor terminal can be expressed as:

$$V_s = \frac{2}{3}(V_{dc} - V_{CF}^{\pm} - \frac{3}{2}L_F \frac{di_m}{dt}) \tag{54}$$

The limit values of inductor L_F and the capacitor C_F can be determined as follows:
During a sampling period T_s, the change in the capacitor voltage can be calculated as:

$$\Delta V_{CF} = \frac{1}{C_F} \int_0^{Ts} i_m dt \tag{55}$$

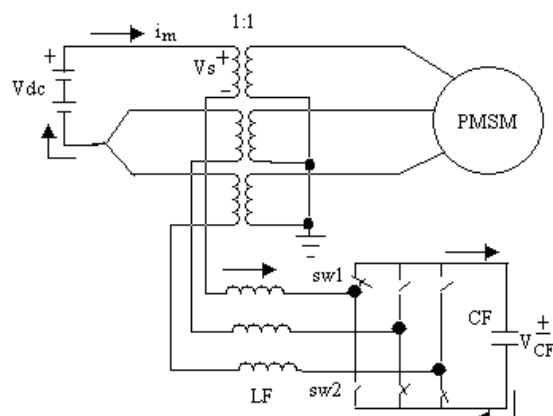So if maximum capacitor voltage change is determined as Vdc, the minimum capacitor value can be calculated as:

Fig. 58. Simplified power circuit of the proposed active filter topology.

$$C_F \geq \left| \frac{\int_{nTs}^{(n+1)Ts} i_m dt}{Vdc} \right| = \left| \frac{Ts \bullet i_{mav}}{V_{dc}} \right| \tag{56}$$

Where, i_{mav} is the maximum of the average current change which can be occurred per sample periods.

The limit values of the smoothing inductance L_F can be expressed as:

$$\frac{1}{(2\pi f_{sw})^2 C_F} < L_F \leq \left| \frac{V_{LFmax}}{\frac{3}{2}\max(\frac{di_m}{dt})} \right| \tag{57}$$

Where, the lower limit is determined by selecting the resonance frequency of the combination $C_F L_F$ to be less than the inverter switching frequency f_{sw} to guarantee reduced switching frequency harmonics. The upper limit is calculated by determining the maximum voltage drop across the inductors V_{LFmax}, and the maximum current change per sampling period di_m/dt.

6.2.4 The Coupling

The coupling between the main inverter circuit and the active filter circuit is achieved through 1:1 transformer, and to attenuate the higher frequency EMI noises, LCR filters are used at the transformer primary and secondary windings as suggested by Fig. 59
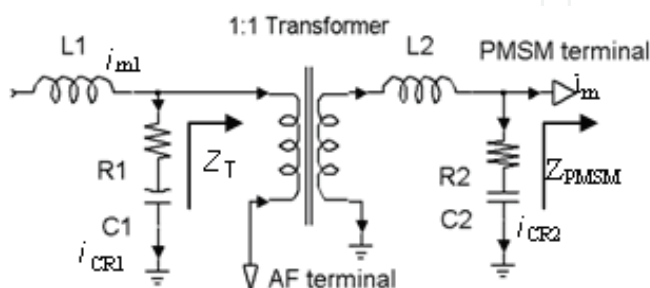

Fig. 59. Coupling between AF and main inverter from one side, and PMSM in the other side.

The important point here is that, the resonance which may arise between capacitor C_1 and transformer primary winding and between capacitor C_2 and motor inductance winding should be avoided when selecting capacitor values.

At selected cutoff frequency, the currents i_{CR1} and i_{CR2} derived by the RLC filters are given by

$$i_{CR1} = \frac{z_T}{z_T + \sqrt{R_1^2 + (1/sC_1)^2}} i_{m1} \quad and$$

$$i_{CR2} = \frac{z_{PMSM}}{z_{PMSM} + \sqrt{R_2^2 + (1/sC_2)^2}} i_{m2} \tag{58}$$

Where, Z_T and Z_{PMSM} are as defined in Fig. 59.

Bearing in the mind the conditions required in the selection of RLC, these currents should be large compared to i_{m1}, drawn by the transformer, and/or i_m, drawn by the motor at selected cutoff frequency; while at operating frequency these currents should be very small compared to i_{m1} and i_m.

6.2.5 Simulation and results

In order to verify that the proposed filter topology does actually improve the performance of the conventional HDTC methods, the HDTC is implemented in Matlab/Simulink to compare the performance of the PMSM with and without the filter topology under the same operating and loading conditions

The motor parameters are in Table 2 and the filters parameters are in Table 6. The AF capacitor used is 200μF and its inductors are 200mH. The drive is IGBT inverter.

L_1	1μH	L_2	1.5μH
C_1	2μF	C_2	2μF
R_1	250Ω	R_2	750Ω

Table 6. Active Filter Topology parameters

The simulation results with 100μs sampling time and ±0.1 Nm hysteresis torque band are shown in Fig. 60 to Fig. 66. The torque dynamic response is simulated with open speed loop, while the steady state performance is simulated with closed speed loop at 70rad/s as reference speed, and 2 Nm as load torque.

The torque dynamic responses before and after connecting the AF are shown in Fig. 60-a and Fig. 60-b respectively. The reference torque for both figures is changed from +2.0 to -2.0 and then to 3.0 Nm. As shown in the figures, the dynamic response with the proposed filter topology is adequately follows the reference torque with lower torque ripples and settles down within ±0.1 Nm band of the reference torque; while the torque dynamic under HDTC without filter topology can not settle down within the specified torque bands due to presence of high torque ripples (± 1.0 Nm). On the other hand, the torque response time without filter topology is shorter (~1.2ms) than the torque response time with the proposed filter topology (2.5ms). This delay in the torque response with the proposed filter topology is mainly due to delay of current propagation through the $L_F C_F$ loop of the active filter however; this is not significant if compared with the results provided by Tang et al (2004).
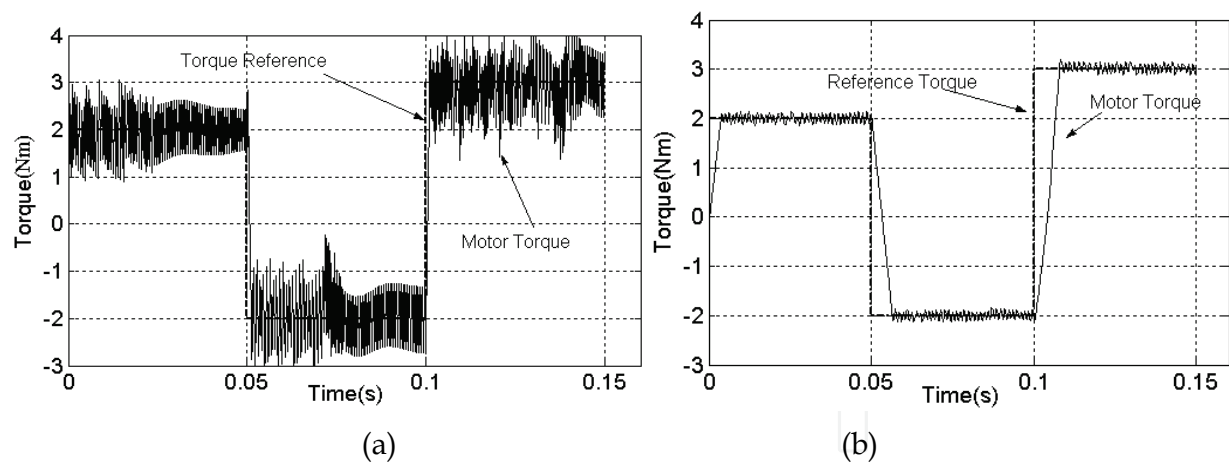
(a)   (b)

Fig. 60. Motor torque dynamic under basic HDTC: (a) before (b) after connecting the AF

The motor steady state performance before and after applying the AF are shown in Fig. 61 to Fig. 64. Fig. 61-a and Fig. 61-b, show the phase voltage provided to the motor terminals before and after applying the filter topology respectively, observe the change of the waveform after applying the AF, it is clear that the phase voltage approaches sinusoidal waveform with almost free of voltage pulses appear in Fig. 61-a due to inverter switching. Better waveform can be obtained by increasing the active filter inductance L_F however, the cost and size of the AF will increase, and therefore suitable inductance value can be selected to achieve acceptable performance. Similar results have been provided by Yilmaz, (Yilmaz et al. 2000), however as compared to above result, their sinusoidal voltage waveform provided to the motor terminals is full of harmonic components.
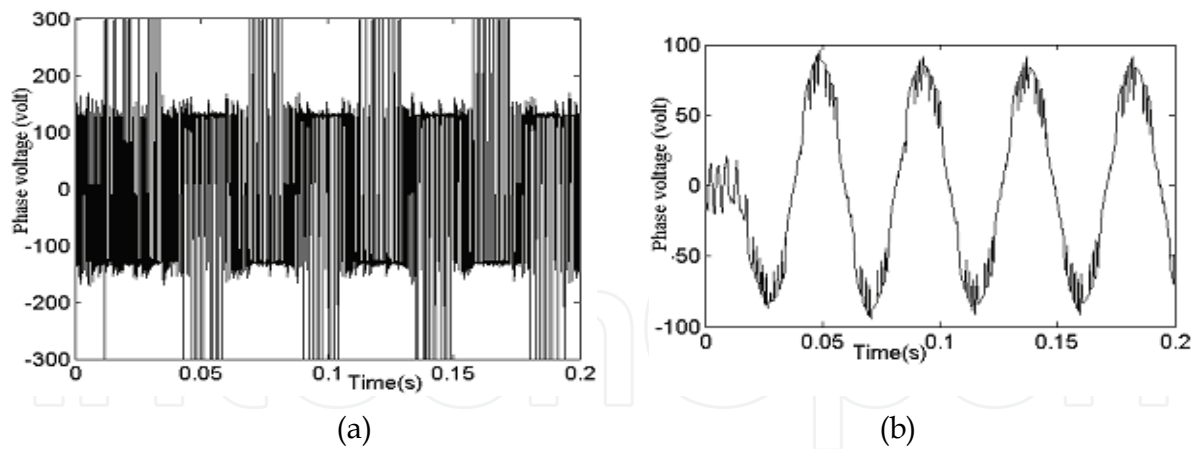

(a)   (b)

Fig. 61. Starting motor phase voltage: (a) before (b) after connecting the AF topology

Fig. 62-a and Fig. 62-b show the response of the motor line currents under HDTC without and with the proposed filter topology respectively. In Fig. 62-a high distortion in line current can be observed, however the current waveform is smoother after applying the proposed filter topology. The reason of the high current distortion (ripples) is mainly due to the fact that switching of the inverter is only updated once at the sampling instances when the hysteresis controllers change state so, with existence of the proposed active filter a proper voltage is provided to the motor terminal which, in turn decreases current ripples.

(a)   (b)
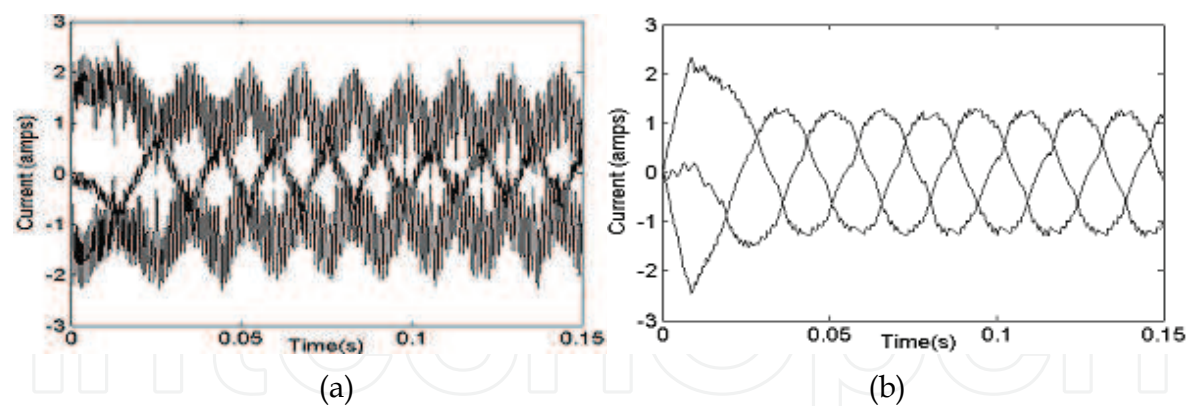
Fig. 62. Motor line currents: (a) before (b) after applying the AF topology.

The torque response in Fig. 63 shows considerable reduction in torque ripples around the load torque when the proposed active filter is connected. The higher ripples of ±1.62Nm around the load torque in Fig. 63-a is mainly due to the existence of harmonic voltages provided to the motor terminals, so when the harmonics are reduced after insertion of the proposed filter topology the torque ripples is decreased down to ±0.1 Nm as shown in Fig. 63-b. The reduction in the torque ripples normally reflected in reduced motor mechanical vibration and hence reduced acoustic noise as well as smoother speed response as shown in Fig. 64.
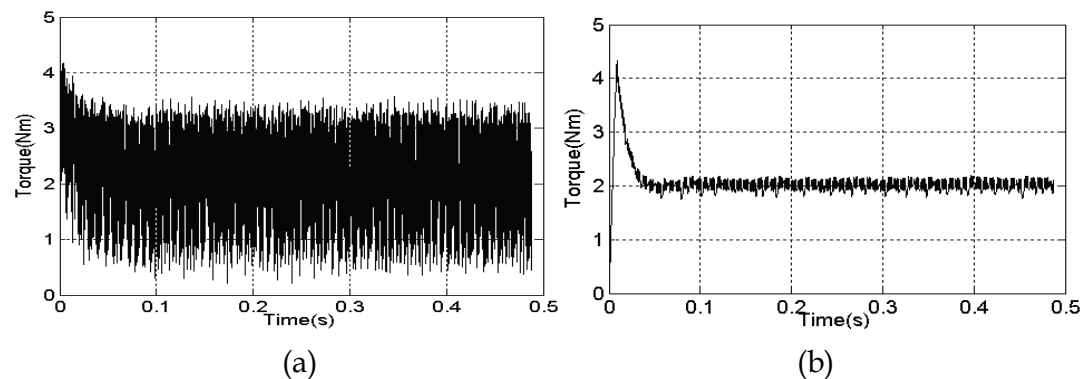

(a)   (b)

Fig. 63. Steady state motor torque response under basic HDTC with 2.0 Nm as load torque (a) before (b) after connecting the AF topology

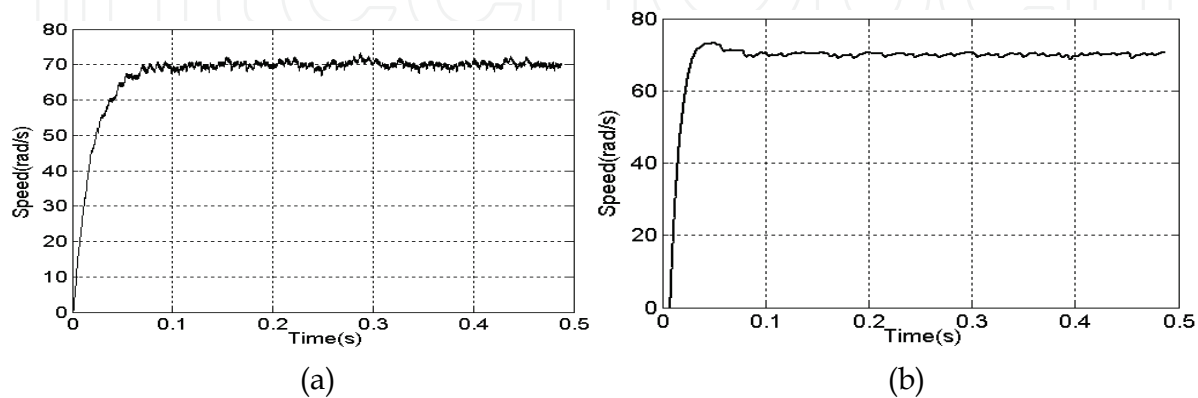(a)   (b)

Fig. 64. Rotor speed under basic HDTC (a)before (b)after applying the AF topology

The status of the phase voltage harmonics and EMI noise in the line currents before and after connecting the AF are shown in Fig. 65 to Fig. 66.

In Fig. 65-a the spectrum of the phase voltage before connecting the AF shows that disastrous harmonic voltages with THD of ~79% have widely scattered in the shown frequency range. These harmonic voltages if not cleared or reduced, it will result in parasitic ripples in motor developed torque and contribute to electromagnetic interference noise, so after connecting the AF, the THD is effectively reduced to less than 5% as in Fig. 65-b.
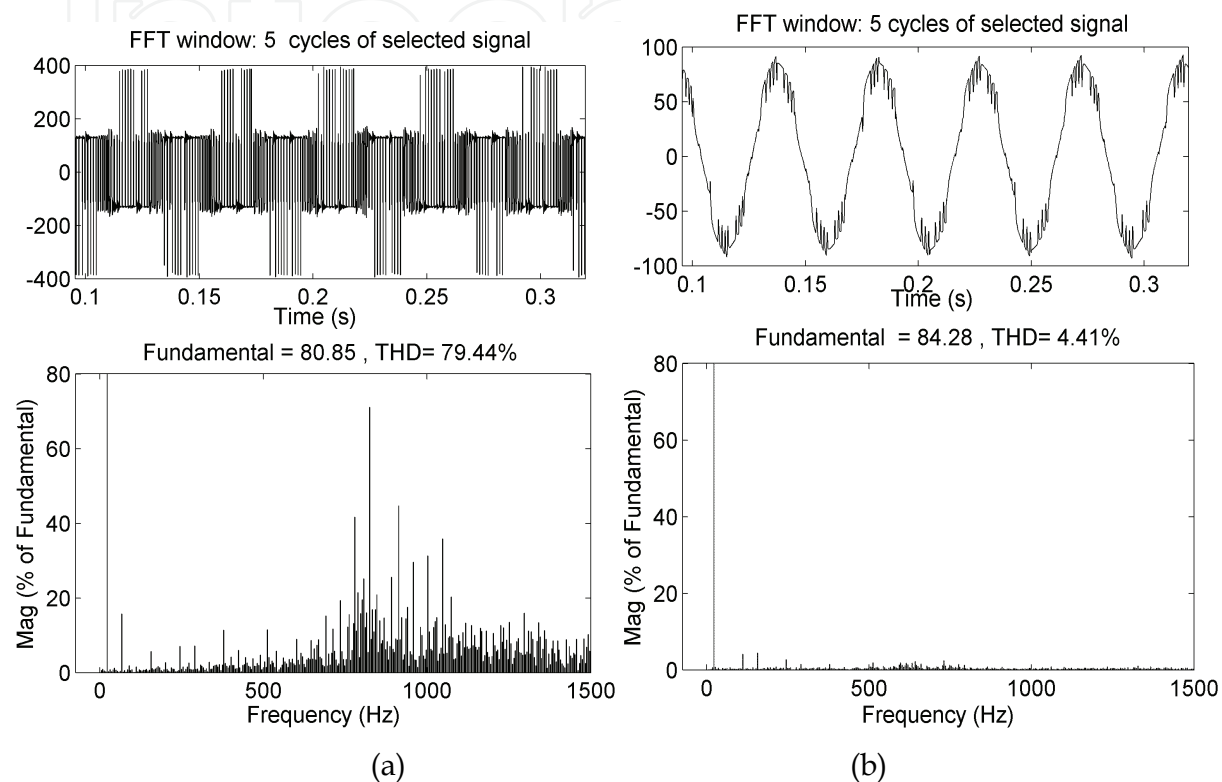
Fig. 65. Phase-a voltage (upper) and it is spectrum (lower):
(a) Before connecting the AF topology   (b) after connecting the AF topology

The EMI noise level before connecting the AF in Fig. 66-a shows a noise level of ~ 20dB at operating frequency, ~18dB at switching frequency (5KHz), and almost -40dBs for the most high frequencies (>0.2 MHz). These noise component frequencies have bad effect on the control system if not filtered. When the AF is connected the EMI noise level is tuned down to ~-18dB at operating frequency, ~-25dB at switching frequency and less than ~-60dBs for the most high frequencies as shown in Fig. 66-b.

From the results presented it can be seen that the steady state performance of the HDTC with the proposed filter topology is much better than the performance presented by Zhong(1997). This result can also be compared with experimental result presented by Tang et al (2004) though the effective average switching sampling time in that method is much less than the selected sampling period (150μs) and that due to the fact space vector modulation was used to drive the inverter.

The motor voltage waveform is better than that provided by Yilmaz, et al(2000), beside the filter topology presented by Yilmaz, et al (2000) is continuously required to be tuned when the switching frequency is changed. In addition in order to obtain acceptable sinusoidal

waveform, the resistor value used in the RLC loop is small, which involves larger current to flow through the loop composed of the RLC and the inverter which in turn causes over loading to the inverter elements.
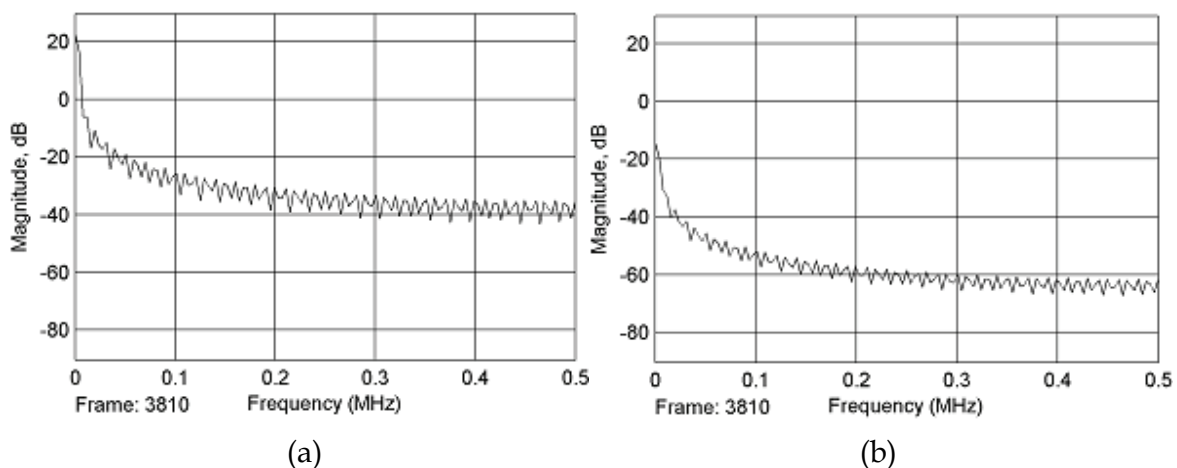

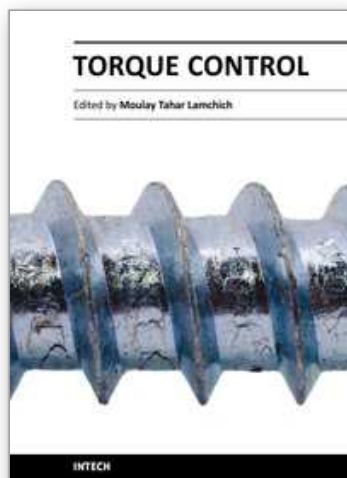Fig. 66. EMI   noise level: (a) before (b) after connecting the AF topology

7. References

Adam A. A. And Gulez K., (2009) "A New Sensorless Hysteresis Direct Torque Control Algorithm for PMSM with Minimum Torque Ripples", COMPEL, Vol.28, No.2, p.p. 437-453, April 2009.

Dariusz, S., Martin, P. K. And Frede, B., (2002),"DSP Based Direct Torque Control of Permanent Magnet Synchronous Motor Using Space Vector Modulation" Proceeding of the 2002 IEEE International Symposium on Industrial Electronics, ISIE 2002 , Vol. 3, 26-29 May , pp. 723-727.

Darwin, R., Morán, L., Dixon, W. J., and Espinoza, J. R,. (2003), "Improving Passive Filter Compensation Performance With Active Techniques," IEEE Transaction on Industrial Electronics, Vol. 50(1), pp. 161-170, Feb. 2003.

Depenbrock, M., (1984), "Direct Self-Control", U.S. Patent, No: 4678248, Oct. 1984.

Depenbrock, M., (1988), "Direct Self-Control of inverter-fed machine", IEEE Transactions on. Power Electronics Vol. 3, No.4, pp. 420-429, Oct. 1988.

Dirk, D., Jacobs, J., De Doncker, R. W. and Mall, H.G.,(2001), " A new Hybrid Filter to Dampen Resonances and Compensate Harmonic Currents in Industrial Power System With Power Factor Correction Equipment," IEEE Transaction on Industrial Electronics, Vol. 16(6), pp. 821-827, Nov. 2001.

Erik, P.,(1992), " Transient Effects in Application of PWM Inverters to Induction Motors", IEEE Transactions on Industry Application, Vol. 28, No. 5, pp. 1095-1101 Sept./ Oct. 1992.

French, C. and Acarnley, P., (1996), "Direct torque control of permanent magnet drives," IEEE Transactions on Industrial Applications., Vol. 32 Issue: 5, pp.1080–1088, Sept./Oct. 1996.

Gulez K., Adam A. A., Pastacı H. (2007), "Passive Filter Topology to Minimize Torque Ripples and Harmonic Noises in IPMSM Derived with HDTC", IJE-International Journal of Electronics, Vol. 94, No:1, p.p.23-33, Jan. (2007).

Gulez K., Adam A. A., Pastacı H. (2008) "Torque Ripples and EMI Noise Minimization in PMSM Using Active Filter Topology and Field Oriented Control", IEEE-Transactions on Industrial Electronics, Vol. 55, No. 1, Jan. (2008).

Hideaki, F., Takahiro, Y., and Hirofumi, A.,(2000), "A Hybrid active Filter For Damping of Harmonic Resonance in Industrial Power Systems,'' IEEE Transaction on Power Electronics, Vol. 15 (2) , pp. 215-222, Mar. 2000.

Holtz, J. and Springob, L.,(1996), "Identification and Compensation of Torque Ripple in High- Precision Permanent Magnet Motor Drives", IEEE Transactions on Industrial Electronics, Vol. 43, No. 2, April 1996, pp.309-320

Hugh, R., Juan, D. and Morán, L., (2003), "Active power filters as a solution to power quality problems in distribution networks", IEEE power & energy magazine Sept./Oct. 2003 pp. 32-40

Jahns, T. M. and Soong, W. L., (1996), "Pulsating torque minimization techniques for permanent magnet AC motor drives – a review," IEEE Transactions on Industrial Electronics, vol. 43, no. 2, pp. 321-330, Feb. 1996.

Jeong-seong, K., Shinji, D. and Muneaki, I.,(2002), "Improvement of IPMSM Sensor less control performance Using Fourier Transform and Repetitive control", IECON 02 Industrial Electronic Society Conference,5-7 Nov. 2002, IEEE, vol. 1 pp. 597-602

Luukko, J.,(2000), Direct Torque Control of Permanent Magnet Synchronous Machines - Analysis and Implementation, Diss. Lappeenranta University of Technology, Lappeenranta, Stockholm, 2000.

Satomi, H., Muneaki, I. and Takamasa, H., (2001), "Vibration Suppression Control Method for PMSM Utilizing Repetitive Control With Auto-tuning Function and Fourier Transform" IECON'01: The 27th Annual Conference of IEEE Industrial Electronics Society, 2001, pp 1673-1679.

Se-Kyo, C., Hyun-Soo, K. and Myun-Joong, Y., (1998),"A new Instantaneous Torque Control of PM Synchronous Motor for High-Performance Direct-Drive Applications", IEEE Transactions on Power Electronics Vol. 13, No. 3.

Springob, L. and Holtz, J., (1998),"High-Bandwidth Current Control for Torque-Ripple Compensation in PM Synchronous Machines", IEEE Transactions on Industrial Electronics, Vol. 45, NO. 5, October 1998, pp.713-721

Takahashi, I. and Naguchi, T.(1998), "A new quick-response and high efficiency control strategy of an induction motor," IEEE Transactions on Industrial Applications, vol. 34, No. 6 pp. 1246-1253, Nov./Dec. 1998.

Tan, Z. Y. and Li, M., (2001), "A Direct Torque Control of Induction Motor Based on Three Level Inverter" , IEEE, PESC'200, Vol. 2 pp. 1435-1439

Tang, L., Zhong, L., Rahman, M. F. and Hu, Y., (2004), "A Novel Direct Torque Controlled Interior Permanent Magnet Synchronous Machines Drive with Low Ripple in Flux and Torque and Fixed Switching Frequency", IEEE Transactions on Power Electronics Vol. 19, No. 2, Mar. 2004

Tang, L., Zhong, L, Rahman, M. F., and Hu, Y., (2001), " A novel Direct Torque Control for Interior Permanent Magnet Synchronous Machine Drive System with Low Ripple In torque and Flux-A Speed Sensor less Approach" IEEE, IAS, 13-18 Oct. 2002, vol. 1, pp.104-111.

Vas, P.,(1996), Electrical Machines and Drives- A Space-Vector Theory Approach, Oxford, USA, 1996.

Yilmaz, S., David, A. T., and Suhan, R., (2000), "New Inverter Output Filter Topology for PWM   Motor Drives", IEEE Transaction on Power Electronics Vol. 15 No 6, pp. 1007-1017, Nov. 2000

Zhong, L., Rahman, M. F., Hu, W.Y. and Lim, K.W., (1997), "Analysis of direct torque control in permanent magnet synchronous motor drives," IEEE Transactions. on Power Electronics, vol. 12 Issue: 3, pp. 528 –536, May 1997.

Torque Control

Edited by Prof. Moulay Tahar Lamchich

This book is the result of inspirations and contributions from many researchers, a collection of 9 works, which are, in majority, focalised around the Direct Torque Control and may be comprised of three sections: different techniques for the control of asynchronous motors and double feed or double star induction machines, oriented approach of recent developments relating to the control of the Permanent Magnet Synchronous Motors, and special controller design and torque control of switched reluctance machine.

How to reference

In order to correctly reference this scholarly work, feel free to copy and paste the following:

INTECH
open science | open minds